Article

Clay Mineralogy: A Signature of Granitic Geothermal Reservoirs of the Central Upper Rhine Graben

Carole Glaas [1,2,3,*], Patricia Patrier [2], Jeanne Vidal [4], Daniel Beaufort [2] and Albert Genter [3]

1. Department ITES UMR 7063, University of Strasbourg, 67084 Strasbourg, France
2. Department IC2MP UMR 7285, University of Poitiers, 86073 Poitiers, France; patricia.patrier@univ-poitiers.fr (P.P.); daniel.beaufort@univ-poitiers.fr (D.B.)
3. ES-Géothermie, 67450 Mundolsheim, France; albert.genter@es.fr
4. Andean Geothermal Center of Excellence (CEGA), Department of Geology, FCFM, University of Chile, Santiago 8320000, Chile; jeannevidal@ing.uchile.cl
* Correspondence: cglaas@unistra.fr

Abstract: Clay minerals are the signature of hydrothermal alterations related to fluid circulation in volcanic and crystalline rocks. In the French part of the Upper Rhine Graben, in the deep-seated granites, illitic minerals (illite and I/S mixed layers (ml)) are typical products of the structurally-controlled argillic alteration in the Paleozoic granitic basement. In the new Illkirch geothermal well, GIL-1, drill-cuttings were studied with various petrographic methods to determine the characteristics of illite in paleo- and present-permeable zones, and to compare the alteration mineralogy with that of geothermal Soultz-sous-Forêts and Rittershoffen sites. Alteration petrography, crystal structure as well as the chemical composition of the illitic minerals and the altered bulk rocks were performed all along the well. This complete characterization, combined with geophysical logs and structural results, highlighted that the illitic minerals at Illkirch, Soultz-sous-Forêts, and Rittershoffen are composed of illite and illite-rich illite-smectite mixed layers (I/S ml) (<10% smectite). Two mineralogical assemblages were distinguished: chlorite + illite resulting from the propylitic alteration after the emplacement of the granitic basement under temperatures higher than 350 °C, and illite + I/S ml + carbonates + quartz resulting from the argillic alteration due to fluid circulation in the fractures at temperatures between 130 and 160 °C. Fracture zones are characterized by the occurrence of illitic minerals (illite and I/S ml), and specifically, by higher quantities of I/S ml in present-day permeable zones than in paleo-permeable zones. A conceptual model of the fracture zones at the interface between the overlying sedimentary rocks and the granitic basement is proposed. The present-day permeability distribution is controlled by the fault and fracture network, which consists of sealed zones and unsealed zones. Fluid convection in the URG implies paleo and present fluids circulating in both fractured sedimentary and crystalline reservoirs. Such circulations develop illitic minerals that could be considered as exploration guides for future geothermal sites in the URG. At Illkirch, the repartition of the present-permeable fracture zones (KFZs) in the GIL-1 well indicates that the moderately argillically altered granite distally situated from the Eschau fault is more permeable than the intensely argillically altered granite close to the Eschau fault.

Keywords: geothermal reservoir; illite; illite-rich illite/smectite mixed-layers; hydrothermal alteration; granite; Upper Rhine Graben

1. Introduction

Geothermal energy is one of the best compromises in terms of low CO_2 emissions among the renewable energy sources [1,2]. An industrially viable project requires a long-life geothermal resource with hot fluids circulating through permeable fracture networks at a drillable depth. In the Upper Rhine Graben (URG), these geothermal conditions are fulfilled: brines (100 g/L, >150 °C) are circulating (optimate flowrate 70 L/s) through a nearly vertical fracture network at the base of the Triassic sedimentary unit and the top

of the Palaeozoic granitic basement (2–3 km depth) [3]. Drilling at the top basement of the fault system at Soultz-sous-Forêts and Rittershoffen led to the successful exploitation of geothermal fractured granite reservoirs. Even if stimulations could contribute to enhance the initial permeability after drilling operations, thereby developing viable enhanced geothermal system (EGS) projects like the Rittershoffen wells [4], the remaining challenge is the implementation of drilling in zones with the best reservoir quality. This requires an understanding of why some fractured zones hosted in granites are more permeable than others. In such granitic geothermal reservoirs, in many places like in Japan, Canada, the United Kingdom, and France, clay minerals have been studied extensively as they are the main products of water–rock interactions like in other high-enthalpy volcanic reservoirs or ore deposits [5–14]. In these various hydrothermal systems, clay minerals are reliable markers of the evolution of the conditions of the hydrothermal system through their mineralogy, their crystal-chemistry, their textural properties as well as their quantity [15]. Illite and illite-rich illite/smectite mixed-layers (namely I/S ml hereafter) constituting both the illitic minerals mentioned in this paper, are typical secondary minerals resulting from the hydrothermal alteration of Al-bearing primary minerals in granites such as feldspars (orthoclase, plagioclase) and ferro-magnesian minerals (biotite, hornblende) [13,16,17]. The formation of illitic minerals is the result of alteration under the condition of high fluid/rock ratio with the dissolution of primary minerals and the creation of significant secondary porosity in fracture controlled damage zones [18–22]. In the case of extreme hydrothermal alteration, the crystallization of illite could also contribute to a partial or total sealing of the secondary porosity and the fault core, contributing to reducing the permeability of the fracture zone. Other secondary minerals associated with illitic minerals, like drusy quartz, carbonates, sulfides, and sulfates may also contribute to the sealing [23]. Several geothermal sites in the URG that have been studied in detail in terms of secondary mineralogy (Soultz-sous-Forêts, Rittershoffen) have reported the occurrence of illitic minerals systematically associated with fracture zones and their damage zones [18,24–26]. These sites show contrasting natural permeability due to the complexity of the fracture zones in terms of structure and secondary mineralogy [4,27]. The aim of this study was to present the secondary mineralogy related to hydrothermal alteration of the granitic rocks in the following geothermal EGS sites: Illkirch, Soultz-sous-Forêts, and Rittershoffen. This study will focus on the alteration parageneses and clay signatures of the fracture-controlled permeable zones of the Illkirch basement. To meet the above objectives, we utilized the following analytical techniques: binocular observations, chemical analyses on bulk rock, x-ray diffraction (XRD), and chemical composition of clay minerals as well as geophysical logs such as temperature log, borehole image log, and gamma-ray (GR).

2. Geological Setting

The geothermal well of Illkirch (GIL-1) was drilled in 2018–2019 and is located a few kilometers south of Strasbourg (Figure 1a). This EGS project located in an urban area was initiated to supply district heating in winter and to produce electricity on the grid in summer from a geothermal doublet. The second well of the doublet will be drilled after injection tests and reservoir studies. Before the drilling of the GIL-1 well, a large exploration campaign was conducted including aeromagnetic and gravimetric surveys as well as a 2D seismic survey [28,29]. The target of the GIL-1 well was to intersect the large-scale Eschau normal fault oriented N10° E at the interface between the Triassic Buntsandstein and the Palaeozoic granite (Figure 1a,b). This target was successfully reached at a 2894 m measured depth (MD) (i.e., 2636 m true vertical depth, TVD). The total depth of the well is 3800 m MD (3391 m TVD) and the open-hole crosses the Buntsandstein sandstone and Carboniferous granite from 2762 m MD (2512 m TVD) to 3800 m MD for a total open-hole length of 1038 m MD (879 m TVD).

The URG is part of the European Cenozoïc Rift System (ECRIS) and is composed of Palaeozoic granites overlaid by Secondary and Tertiary sediments (Figure 1). Its morphology is today still controlled by NNE–SSW normal faults and fractures that are the trace

of its tectonic activity. Within the URG, gravity and magnetic data delineated intrusive granitic bodies resulting from a magmatic activity of the late-Variscan age. Such intrusions were confirmed by deep drilling and they were classified as porphyritic monzogranite and two-mica granite, both of which were observed at Soultz-sous-Forêts and Rittershoffen. Geochronological data indicate that the massive porphyritic monzogranite and the two-mica granite were emplaced and cooled down at 333 and 327 Ma, respectively [30,31]. Upon granite emplacement, the granitic bodies first underwent a pervasive and widespread propylitic alteration, which transformed primary minerals to secondary chlorite, carbonates, and epidote [31] at temperatures higher than 350 °C [32]. The next argillic alteration, characterized by illite and illite-smectite mixed layers, carbonates, euhedral quartz, and sulfides, was controlled by fracture networks (Figure 1c). The structural and hydrothermal histories of the URG lead to several argillic events (Figure 1c). However, dating of illite is rare and shows scattered ages, showing that this alteration type recurred in several episodes from the Permian to Cretaceous [33,34]. Fluid inclusion studies have indicated that this argillic alteration occurred at 130–160 °C, and that a deep penetration and large scale fluid movements took place between the sedimentary cover and the granitic basement [32]. Within a fractured zone, six generations of euhedral quartz were observed and interpreted as the short pulses of hydrothermal fluid flow through the fracture network possibly due to seismic reactivations [35]. So far, dating has not been determined for the Illkirch granite, and therefore it is not possible to address the timing of the hydrothermal events. The geological section presents two main unconformities: the Permo-Triassic and Paleocene unconformities that reflect large-scale deformation with subsidence, uplift, and erosion [36].
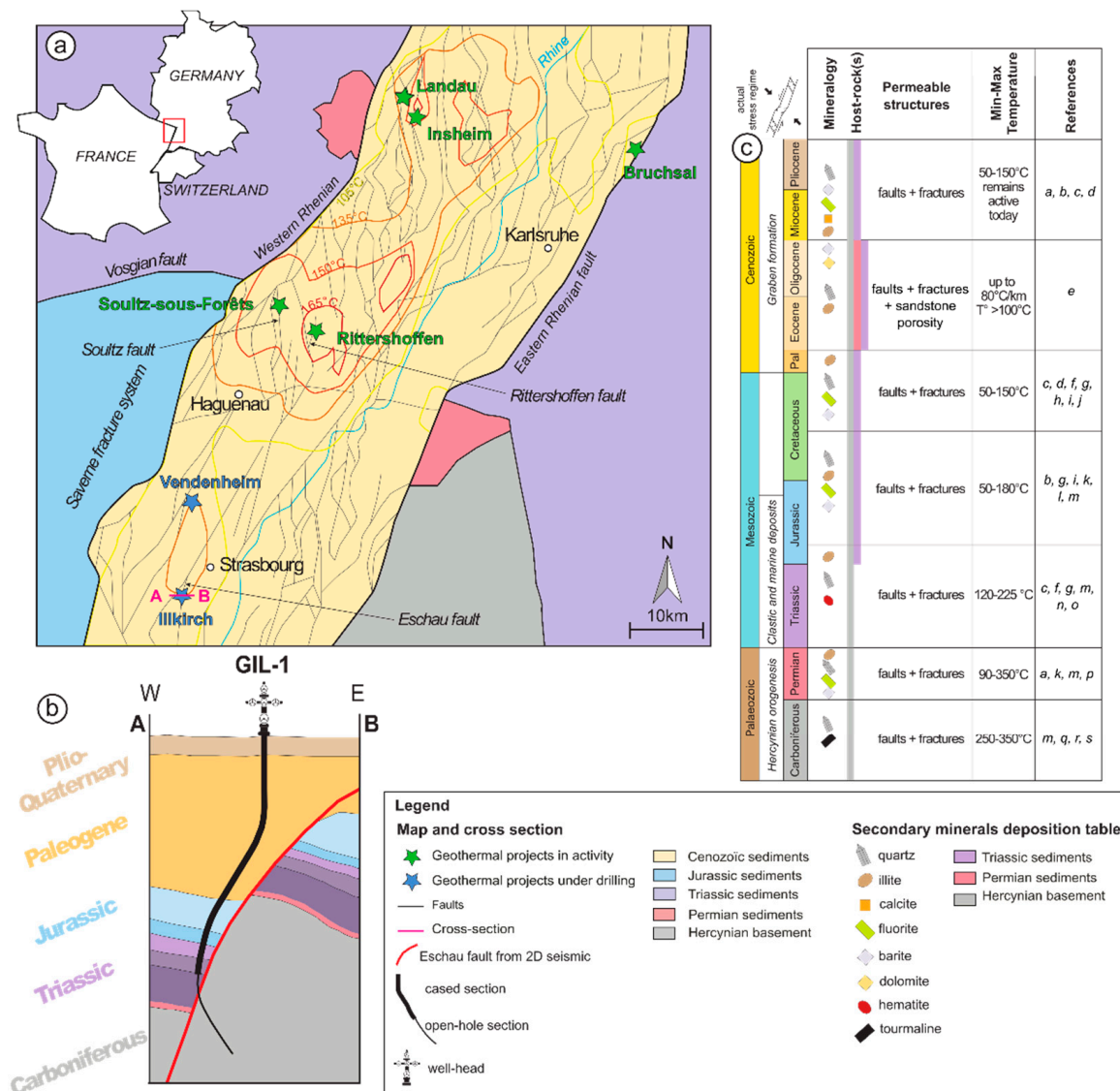
Figure 1. (**a**) Structural and geological map of the central URG with isotherms at a 2 km depth from the geoportal GeORG [37]. The location of the geothermal power plants in exploitation and under drilling is also shown; (**b**) cross section through the Illkirch site showing the GIL-1 well trajectory through the sedimentary layers, the Eschau fault, and the granitic basement (**c**) episodes of secondary mineral deposition occurring in the URG are presented along the geological timescale from the Palaeozoic to the Cenozoic ages, modified after [38]. References in (**c**) are (a) [39], (b) [40], (c) [41], (d) [34], (e) [42], (f) [43], (g) [44], (h) [45], (i) [46], (j) [47], (k) [33], (l) [48], (m) [49], (n) [50], (o) [51], (p) [52], (q) [53], (r) [54], (s) [55].

Deep fluids in the geothermal reservoirs of Soultz-sous-Forêts and Rittershoffen are of the NaCl type with total dissolved solid (TDS) values close to 100 g/L (Table 1) [56,57]. The pH values of the fluids in the reservoirs are close to 5.0 [57] (Table 1). Fluids at Landau, Insheim, Soultz-sous-Forêts, and Rittershoffen show a similar chemical composition [56,58]. The geochemical characteristics of the fluids were interpreted based on the chemical analyses for both major and trace elements in the water samples, and the isotopic analyses of the water samples (δD and δ^{18}O of the water, δ^{18}O and δ^{34}S of the dissolved sulfate, δ^{13}C of the dissolved carbonate, and the δ^{7}Li, δ^{11}B, and ^{87}Sr/^{86}Sr), [56,58]. The fluid composition is controlled by the mixing between the recharge of meteoric water along the normal border faults and the primary marine brine [56,58,59].

Table 1. Chemical compositions of the geothermal fluid sampled in the Palaeozoic granite reservoir at Soultz-sous-Forêts in the GPK-2 well (05.02.2020) and at Rittershoffen in the GRT-1 well (04.11.2020) [57].

Geothermal Site	T_{Bottom} °C	pH	TDS g/L	Na mg/L	K mg/L	Ca mg/L	Mg mg/L	Cl mg/L	SO_4 mg/L	SiO_2 mg/L	Br mg/L	Li mg/L	Gas
Soultz-sous-Forêts	200	4.98	99	26,400	3360	7020	123	55,940	108	179	240	160	CO_2 N_2 CH_4
Rittershoffen	>160	6.27	101	27,960	3890	7450	111	65,030	76	175	247	203	CO_2 N_2 CH_4

Biotite compositions from the propylitically altered granite of Soultz-sous-Forêts, Rittershoffen, and Illkirch plot in the subalkaline association of the magnesium-potassium field (Figure 2) show geochemical compositions similar to those of the outcropping granites of the Crêtes and of the Mayet-de-Montagne located in the Vosges Massif and the French Massif Central, respectively [60–62] (Figure 2). The biotites of Rittershoffen are less magnesian than those of Soultz-sous-Forêts, like late Variscan granites (Figure 2).

The complex tectonic history of the URG was accompanied by several hydrothermal events, which produced secondary minerals that are the records of the paleo-thermal and chemical conditions of the system [38,42]. The fluid mostly circulates through the local normal faults and their associated small-scale fracture networks at the sedimentary layers–basement interface (Figure 1) through convection cells [63]. Consequently, this results in the formation of several localized temperature anomalies in the URG. The Illkirch project was designed to take advantage of the Strasbourg temperature anomaly (Figure 1a). The secondary minerals are mainly composed of quartz and carbonates, in addition to clay minerals (Figure 1c). In Illkirch, the argillic alteration is likely related to the past activity of the Eschau fault (Figure 1b) [31,32]. Moreover, the dissolution features of the propylitic chlorite and its replacement by illite (argillic illitization) evidence the postdating of propylitic alteration by argillic alteration.
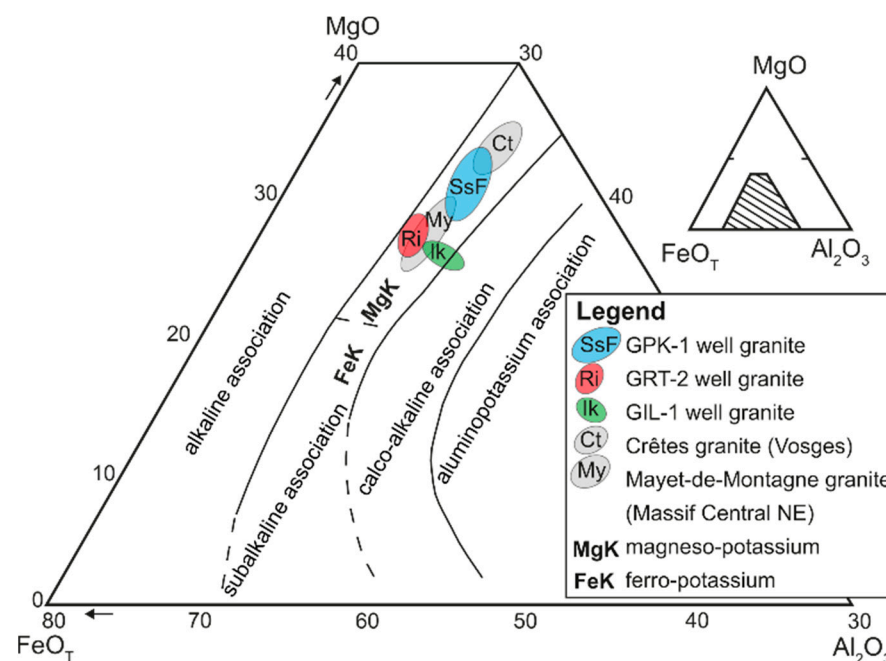

Figure 2. Compositions of biotite in basement rocks from Soultz-sous-Forêts (SsF), Rittershoffen (Ri), and Illkirch (Ik) in the Upper Rhine Graben compared to those of biotite from the Crêtes and Mayet-de-Montagne granites in the MgO, FeO, and Al_2O_3 diagram after [60–62].

3. Materials and Methods

A detailed petrographic and mineralogical characterization of the granitic reservoir was conducted based on laboratory analyses on cuttings samples and geophysical logs, with the aim to characterize the mineralogical signature of permeable zones.

3.1. Binocular Observations on Cuttings

The cuttings (chip samples) collected during the rotary drilling of the GIL-1 well at Illkirch were first washed using sieves and then dried on-site in an oven at 80 °C for 40 min by the mud logger crew. The cuttings were sampled at every 5 m depth intervals in the 8 1/2″ and 6″ drilled sections. Thus, each sample represents approximately 0.1 m^3 of drilled rock in the 6″ section and 0.16 m^3 of drilled rock in the 8 1/2″ section. The average grain size of the cuttings in each sample varied between 0.5 and 2 mm. The cuttings were observed with a binocular magnifier on-site during the drilling. The presence and abundance of each primary and secondary mineral were initially estimated with a scale of three classes from 0–30, 30–70, and 70–100% to build a petrographic log (Figure 3) representing the hydrothermal alteration grades according to previous studies on Soultz-sous-Forêts and Rittershoffen wells [24,64,65].

3.2. Geophysical Logs

3.2.1. Gamma Ray

The GR log is indicative of natural radioactivity (cumulative emissions, mainly from uranium (U), potassium (K), and thorium (Th)) in gAPI (American Petroleum Institute); GR measurements of the GIL-1 well were performed every 2.5 cm (Figure 3). The GR log is aimed at interpreting lithology and rock composition by detecting clay minerals rich in potassium (mainly illite). In the altered crystalline basement, negative GR anomalies may reflect the occurrence of drusy quartz veins in the host rock [18,66]. Generally, the GR data are an indicator of hydrothermal alteration and thus provide information regarding paleo-permeability.

3.2.2. Temperature

Thermal anomalies identified on temperature profiles are interpreted as the signatures of present-day fluid circulations between the well and the formation and thus reflect the present-permeable fracture zones (KFZs) [67–71]. In the GIL-1 well, the temperature profiles of the open hole section were acquired inside the drill strings due to various technical constrains. Because of time constrains during drilling operations, it was not possible to wait until thermal equilibrium to run the temperature profiles. Therefore, in order to help identify the permeable zones, the temperature logs were performed only several hours after substantial cold-water injections. Using this method, the permeable zones cooled down by the injections appear as negative thermal anomalies on temperature profiles (after a short heating period) (Figure 3). The thermal anomalies seem to be influenced by the absence of thermal equilibrium rather than the fact that they were acquired in the drill strings. In the GIL-1 well, one temperature anomaly was identified in the Buntsandstein sandstone and six were identified in the granitic section (Figure 3). These temperature anomalies are hereafter named the present-KFZs, as opposed to the paleo-KFZs that largely designate all the zones affected by argillic alteration and do not exhibit temperature anomalies (Figure 3).
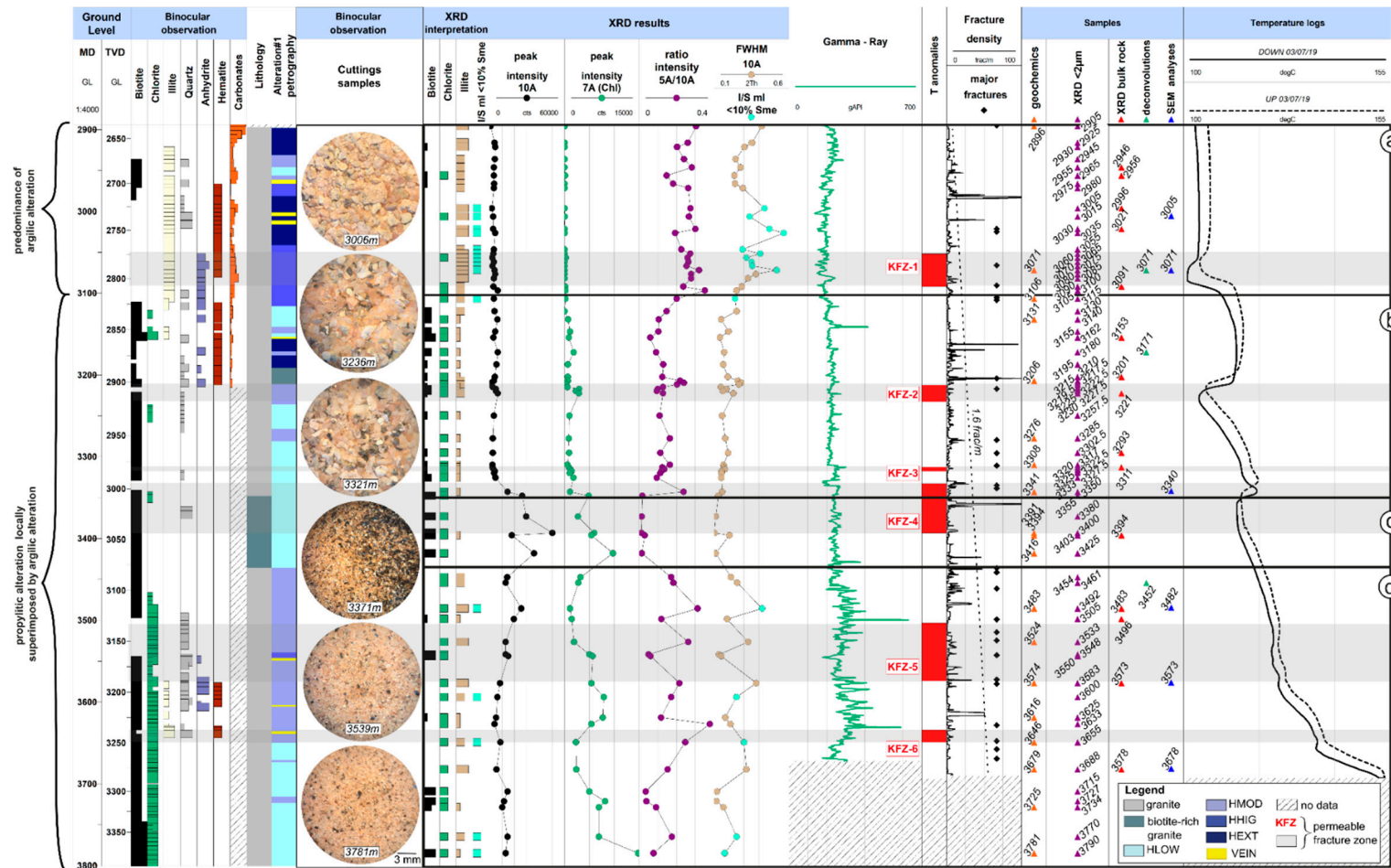
Figure 3. Composite log from the lower part of the open-hole of the GIL-1 well granitic basement, presenting from left to right: the petrographic log built from the binocular lens observations; the XRD results from the oriented Figure 5 and their interpretation; the gamma-ray log; the permeable zones; the fracture density; the major fractures and the samples for which deconvolution of the peak at 10 Å, and SEM analyses were performed. HLOW, HMOD, HHIG, and HEXT: low, moderate, high, and extreme argillic alteration, VEIN: secondary drusy quartz veins, KFZ: permeable fracture zones. The granitic basement is divided in four depth sections that correspond to the grade of hydrothermal alteration and the lithology as follows: (**a**) intense argillic alteration; (**b**) propylitic alteration locally superimposed by argillic alteration; (**c**) fresh biotite-rich graniteand (**d**) propylitic alteration locally superimposed by argillic alteration.

3.2.3. Fractures from Borehole Images

The fractures were extracted from electrical image logs acquired in the open-hole section of the GIL-1 well. Then, the major fractures were selected on the basis of the following criteria:

- The aperture corrected from the borehole orientation >10 mm;
- The resistivity <2000 ohm·m on the induction log; and
- The conductive contrast on the electrical image logs.

The fracture density curve is also presented in Figure 3.

3.3. Chemical Analyses on Bulk Rock

Nineteen cuttings samples were selected in the granitic section of the GIL-1 well, covering the several alteration facies and permeable zones, for chemical analyses of major oxides. Chemical analyses were conducted at the CRPG laboratory in Nancy (France). Samples with cutting sizes larger than 1 mm were ground. Analyses of the major element oxides (SiO_2, Al_2O_3, Fe_2O_3, MnO, MgO, CaO, Na_2O, K_2O, TiO_2, P_2O_5) were carried out on samples initially melted in $LiBO_2$ and put in acidic solution. Analyses were done with an ICP-OES instrument [72]. These chemical analyses were performed in order to follow the chemical differences between the several alteration grades (Table 2).

Table 2. Chemical compositions of major element oxides of 20 cuttings samples from the GIL-1 well. Samples are sorted by facies and grade of alteration. GRBT: Biotite-rich granite, HLOW, HMOD, HHIG and HEXT: low, moderate, high and extreme argillic alteration, respectively. VEIN: secondary drusy quartz veins.

Depth MD	Facies and Alteration	SiO_2 (%)	Al_2O_3 (%)	Fe_2O_3 (%)	MnO (%)	MgO (%)	CaO (%)	Na_2O (%)	K_2O (%)	TiO_2 (%)	P_2O_5 (%)	LOI (%)	Total (%)
3391 m	GRBT	66.89	13.91	4.24	0.14	1.99	1.98	2.78	4.77	0.59	<L.D.	2.02	99.32
3394 m	GRBT	69.07	14.17	3.14	0.11	1.48	2.07	2.99	4.65	0.42	<L.D.	1.94	100.02
3416 m	GRBT	65.94	14.23	4.52	0.15	2.45	1.81	2.87	4.73	0.65	<L.D.	2.26	99.62
	MEAN GRBT	67.30	14.10	3.97	0.13	1.97	1.95	2.88	4.72	0.55	<L.D.	2.07	97.58
3131 m	HLOW	65.39	15.23	2.32	0.10	1.20	3.36	2.73	5.28	0.25	<L.D.	4.03	99.88
3308 m	HLOW	65.83	17.13	2.55	0.08	1.09	3.00	4.11	4.44	0.33	0.11	1.54	100.20
3341 m	HLOW	70.38	11.04	2.51	0.07	0.73	2.75	1.54	4.62	0.29	<L.D.	4.85	98.77
3679 m	HLOW	69.95	12.74	2.13	0.08	0.91	2.19	3.60	4.46	0.21	<L.D.	4.14	100.40
3781 m	HLOW	72.94	13.08	2.16	0.09	0.82	1.89	2.77	4.68	0.23	<L.D.	2.04	100.69
	MEAN HLOW	68.90	13.84	2.33	0.08	0.95	2.63	2.95	4.70	0.26	0.11	3.32	96.67
3276 m	HMOD	65.48	16.47	2.64	0.08	1.18	2.78	3.84	4.62	0.34	0.11	2.06	99.59
3483 m	HMOD	70.39	12.27	1.95	0.08	0.94	2.75	1.00	5.66	0.23	<L.D.	4.14	99.41
3524 m	HMOD	72.77	11.90	1.87	0.07	0.88	2.36	0.81	5.38	0.22	<L.D.	4.05	100.31
3574 m	HMOD	69.43	12.26	2.11	0.09	1.10	2.00	3.11	4.89	0.29	<L.D.	4.42	99.69
3644 m	HMOD	71.35	13.14	2.11	0.07	0.84	1.96	2.13	5.17	0.25	<L.D.	3.52	100.53
	MEAN HMOD	69.88	13.21	2.14	0.08	0.99	2.37	2.18	5.14	0.27	<L.D.	3.64	96.27
3725 m	HMOD/VEIN	73.61	13.24	1.75	0.06	0.70	1.43	3.22	4.67	0.20	<L.D.	1.86	98.89
3071 m	HHIG	60.36	14.75	2.90	0.15	1.81	4.74	1.79	6.07	0.22	<L.D.	7.36	100.16
3106 m	HHIG	65.25	13.32	2.46	0.11	1.50	3.96	1.75	5.58	0.20	<L.D.	5.76	99.90
3206 m	HHIG	61.76	14.47	5.35	0.11	1.11	3.91	2.16	5.14	0.27	<L.D.	5.37	99.65
	MEAN HHIG	62.46	14.18	3;57	0.13	1.48	4.20	1.90	5.60	0.23	<L.D.	6.16	93.74
2896 m	HEXT	59.66	2.57	1.52	0.29	0.96	17.61	0.05	1.31	0.06	<L.D.	15.68	99.71
3006 m	HEXT/VEIN	64.27	14.72	2.42	0.10	1.08	3.70	1.45	5.90	0.24	<L.D.	6.06	99.94

3.4. X-ray Diffraction

XRD analyses were carried out on granitic cuttings of the GIL-1 well to identify the clay minerals and associated secondary minerals. The sampling was concentrated in the permeable and altered fracture zones (FZs) as well as in the unaltered monzogranite (GRAN), and biotite-rich granite. Fifteen samples were also selected to analyze the bulk rock mineralogy. These 15 cuttings were grounded with an agate mill and prepared as disoriented powders. Analyses were carried out on a Phillips X'Pert Pro (Panalytical B.V., Malvern, UK) diffractometer (CuKα radiation, 40 kV, 40 mA). The analytical conditions were as follows: angular domain: 2–65° 2θ; step increment: 0.0235 2θ; and counting time

per step: 0.90 s. Seventy-one cuttings were used for clay mineral identification and were dispersed in distilled water by ultrasonic vibration without any preliminary grinding to avoid contamination of the <5 μm fraction by primary micas. Oriented powders were prepared from the <5 μm fraction size separated from suspension in water by sedimentation. Clay minerals were identified by XRD of the air-dried (AD) and ethylene-glycol (EG)-saturated oriented powders carried out on the same diffractometer. The analytical conditions were as follows: angular domain: 2–35° 2θ; step increment: 0.0235 2θ, and counting time per step: 0.73 s. XRD data acquisition and treatment were conducted using the X'Pert HighScore software (PANalytical B.V.) at the IC2MP laboratory at the University of Poitiers, France. X-ray identification of clay minerals, which is based on the d-values and the relative intensity of their 00*l* reflections, was undertaken with reference to the works of [73,74]. After background stripping, the peak profiles of illite-like minerals were decomposed in the range 6–11° 2θ, as a sum of Gaussian curves using the Fityck software [75].

3.5. Optical Microscope and Scanning Electron Microscope Coupled with Energy Dispersive Spectroscopy

Seven samples were selected in the granitic section to prepare polished thin sections for scanning electron microscope (SEM) analyses. These seven samples were composed of six cuttings and one rock sample of which its depth is unknown as it came to the surface within the drilling tools. These seven polished thin sections were first observed with an optical microscope to previously select microsites for SEM analyses (Figure 4). These samples were selected to cover permeable and non-permeable zones as well as the several alteration grades of the granite:

- in two permeable zones at 3071 m and 3340 m,
- in four non-permeable zones at 3005, 3482, 3573, and 3678 m,
- in the HEXT grade at 3005 m,
- in the HHIG grade at 3071 m,
- in the HMOD grade at 3482 and 3573 m, and
- in the HLOW grade at 3340 and 3678 m.

For the six cuttings samples, the thin sections were made of grains in a resin matrix, thus the texture of the rock as well as the continuity of veinlets was lost. The SEM observations were conducted on a JEOL JSM-IT500 SEM equipped with a BRUKER linxeye energy dispersive spectrometer (EDS) associated with SPIRIT software at the IC2MP laboratory, University of Poitiers, France. These analyses were conducted in order to obtain chemical composition of preselected minerals. The analytical conditions were as follows: 15 kV; 1 nA; counting time: 50 s; and working distance: 11 mm. Analyses were calibrated using natural standards: albite for Na, Al, Si; almandine for Fe, Mg; diopside for Ca, orthoclase for K; spessartine for Mn and Ti metal for Ti and corrected by the PhiRhoZ method. Before measurement, thin sections were coated with carbon.
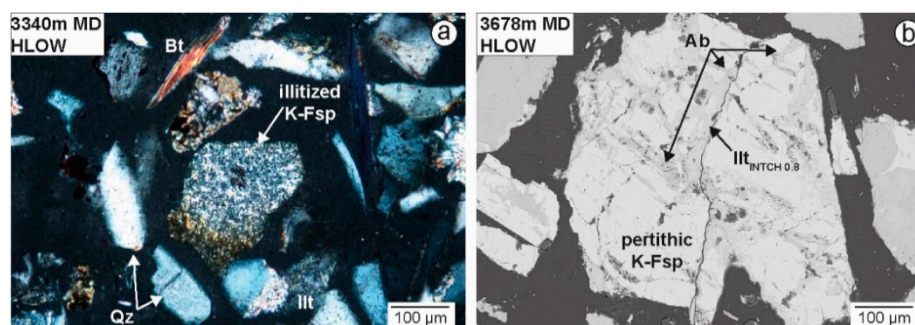

Figure 4. *Cont*.
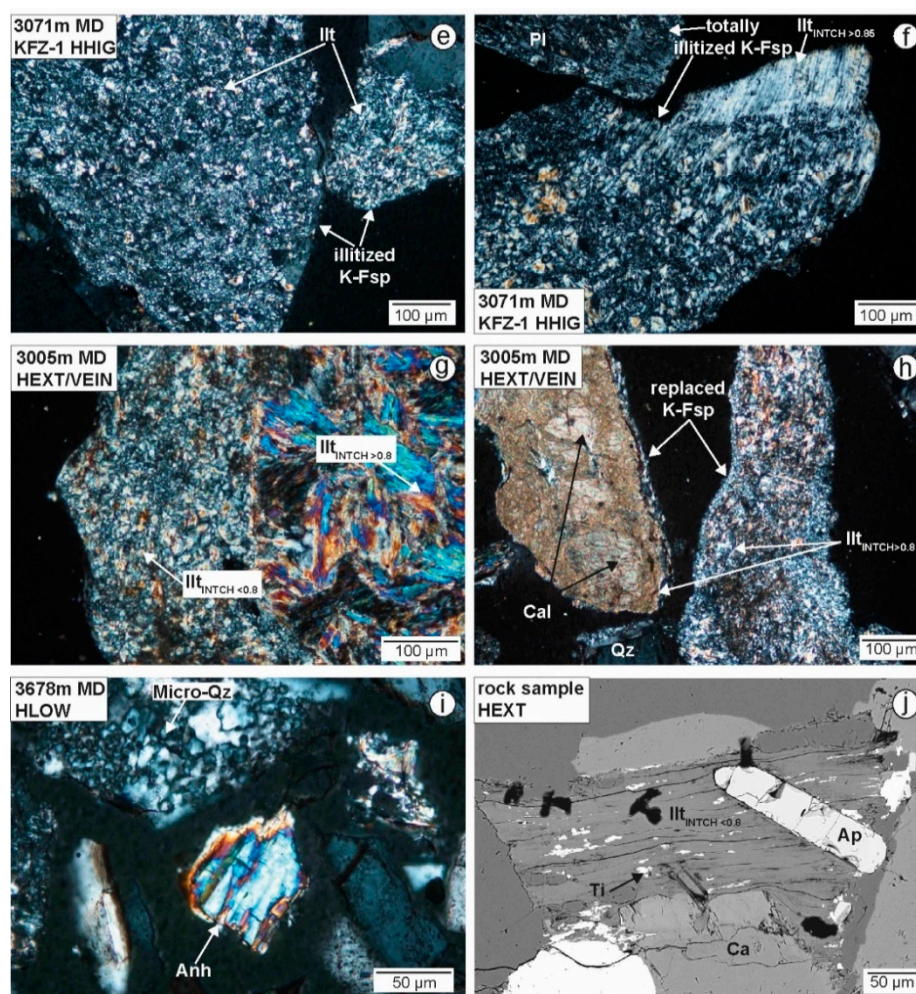
Figure 4. Microscopic observations of thin sections of cuttings (**a–i**) and rock sample (**j**) fixed in epoxy in GIL-1 at (**a**) 3340 m MD (crossed polarized light, CPL), (**b**) 3678 m MD (SEM observations), (**c**) and (**d**) 3482 m MD (CPL and SEM), (**e**) and (**f**) 3071 m MD (CPL), (**g**) and (**h**) 3005 m MD (CPL), (**i**) 3678 m MD (CPL), (**j**) unknown depth (SEM). Anh = anhydrite, Ap = apatite, Bt = biotite, Cal = calcite, Ilt = illitic minerals, K-Fsp = potassic feldspar, Pl = plagioclase, Qz = quartz, Ti = non identified titanium oxide; INTCH = interlayer charge; HLOW, HMOD, HHIG, and HEXT = low, moderate, high, and extreme argillic alteration, respectively.

4. Results

4.1. Petrographical Log—Mineralogy

Two types of granite were crosscut by the GIL-1 well. First, a porphyritic monzogranite containing biotite, oligoclase, perthitic orthoclase, and quartz corresponded to the porphyritic monzogranite encountered in the Soultz-sous-Forêts and Rittershoffen wells, which was named "GRAN" [65,76]. Second, a biotite-rich granite was also encountered at a depth interval between 3346 and 3433 m MD. Argillic alteration is pervasive in the upper part (from 2894 to 3104 m MD, Figure 3a) of the drill hole whereas propylitic alteration occurred mostly in the bottom part (from 3104 to 3800 m MD, Figure 3b,d). Nevertheless, weak argillic alteration was also observed around permeable fractures in the granitic basement (Figure 3b,d). On the basis of petrographic and mineralogical considerations, we can divide the petrographic log into three different domains.

The first one corresponds to granite between 3104 and 3350 m MD and between 3433 and 3801 m MD (Figure 3b,d), in which pervasive propylitic alteration has been overprinted only locally by argillic fracture-controlled argillic alteration. Illitic minerals associated with quartz veinlets (VEIN) and anhydrite infilled the fractures (Figure 3b,d and

Figure 4i) and feldspars were variably replaced by illite in wallrocks (Figure 3a–d). Apatite was also locally observed, associated with chloritized and illitized biotites with Ti-oxide inclusions (Figure 4j). Calcite was not recorded below 3200 m MD, but we cannot exclude its presence under the form of local veins in the vicinity of permeable fractures. Large size illite crystals (10–20 μm, Figure 4d) appear to have crystallized earlier than the fine grained illitic matrix and could be related to the propylitic alteration event [24,25,33,34,62,77–80]. The presence of two populations of illitic minerals based on their crystal size suggests that at least two alteration events affected these primary minerals. In addition to these large size illitic phases, the propylitic alteration consists of disseminated secondary Fe-Mg chlorite, which crystallized as replacement of the igneous biotites. Nevertheless, relicts of primary biotite are still visible in some places (Figure 5a). This pervasive chloritization did not precipitate from the fluids, and is not spatially related to fractures or veins, but occurs essentially as a biotite pseudomorph in association with inclusions of Ti-oxides and micro-lens of carbonates, feldspars, and quartz. These observations characterize the slightly and moderately altered granite (low and moderate hydrothermal alterations, respectively: HLOW and HMOD).

The second petrographic domain is related to an intense argillic alteration observed all around the past and present permeable fractures. This alteration dominates at the upper granite (2894 to 3104 m MD) with very high amounts of illitic minerals in the core of faults as well as in the surrounding damage zones, where it infills fractures in the fault gouge and secondary pores formed by dissolution of feldspars and chlorite in the altered wall-rocks (Figure 3a). Based on crystal size, two populations of illite can be recognized (Figure 4f–h), among which a fine grained illitic matrix is predominant (<5 μm, Figure 4e–h). Secondary hematite and anhydrite (Figures 3a and 4i) as well as drusy quartz (VEIN) are observed locally in small amounts (Figure 4a,i). Calcite is present in substantial amounts (Figure 3). This second domain reflects a granite highly and extremely altered (+/− HMOD, high and extreme hydrothermal alterations, respectively, HHIG and HEXT).

The third petrographic domain corresponds to the fresh biotite-rich granite. Preservation of primary biotite and muscovite evidence an unaltered granite rich in biotite (Figure 3c). This biotite-rich granite is observed from 3350 to 3433 m MD.

4.2. Geophysical Logs

4.2.1. Gamma-Ray

The top of the granite (from 2900 to 2940 m MD) was characterized by high values around 230 gAPI, plausibly due to the abundance of illite at the faulted interface between sandstone and granite (Figure 3). In the intense argillic alteration domain that extends from 2940 to 3100 m MD, the GR values were around 190 gAPI. At deeper zones from 3100 to 3433 m MD, the GR values oscillated between 225 and 245 gAPI in both domains of propylitic alteration and fresh biotite-rich granite. Then, in the deepest part, the GR values were very disturbed, showing two hips from 3450 to 3530 and from 3560 to 3670 m MD where the values oscillate between 180 and 511 gAPI. Below this zone, the GR was not measured. Generally, the GR intervals fit well with the vertical distribution of the different mineralogical assemblages as defined previously (Figure 3). However, in the Illkirch well, no clear correlation exists between the grade of alteration and the GR values.

4.2.2. Permeable Fracture Zones

Twenty-seven major fractures were identified in the granitic section (Figure 3). In addition to these major fractures described above, smaller-scale fractures were also observed on electrical image logs. The density of fractures measured in the Illkirch well (average 1.6 frac/m) was higher than that measured with equivalent techniques of electrical and acoustic borehole images in the Soultz-sous-Forêts (average 0.6 frac/m) and Rittershoffen (average 0.7 frac/m) wells. In the granitic open-hole of the GIL-1 well, six temperature anomalies were interpreted as permeable zones and were linked to major fractures observed on the electrical borehole images. These KFZs are numbered as follows (Figure 3):

- KFZ-1 from 3050 to 3090 m MD,
- KFZ-2 from 3210 to 3230 m MD,
- KFZ-3 from 3310 to 3315 m MD,
- KFZ-4 from 3330 to 3390 m MD,
- KFZ-5 from 3500 to 3570 m MD,
- KFZ-6 from 3630 to 3645 m MD.

Only one (KFZ-1) was in the granite strongly affected by vein alteration and the five other KFZs were located in the granite affected predominantly by propylitic alteration but were generally close to quartz veins or the HMOD alteration grade. The particularity of KFZ-4 is its position at the interface between the pervasively altered granite and the fresh biotite-rich granite (Figure 3b,c). It appears that the occurrence of KFZ is systematically associated with the occurrence of clusters of major fractures (Figure 3), regardless of fracture densities.

4.3. Bulk Rock Chemical Composition

The chemical compositions of the bulk rock major element oxides on bulk rock are presented in Table 2. The loss of ignition (LOI) value includes H_2O (corresponding to hydroxyl group of clay minerals), and CO_2 corresponding to carbonates. We observed that the LOI values increased with the hydrothermal alteration grades (Table 2). This observation was generally valid for all samples except for quartz vein-bearing alteration zones at 3005 and 3724 m MD (Table 2). Considering that LOI is due to the dehydroxylation of the clay minerals (5.5–13% H_2O, according to [81]) and the decarbonation of calcite (44% of CO_2), and that calcium is mostly contained in the calcite, then it is possible to estimate the LOI value reflecting only the secondary clay minerals (illite and chlorite). Hence, the Ca amount in primary feldspars can be neglected because CaO in oligoclase is between 3 and 5% and as feldspars represent 19% of the granite mass. When the samples are hydrothermally altered, the CaO and K_2O values in mass % increase, reflecting the presence of carbonates and illite. SiO_2 value in mass % varies according to the frequency of quartz veins intersected. The mean LOI value for unaltered biotite-rich or porphyritic monzogranite or even HLOW is 2%, for HMOD it is around 4%, and for HHIG, it is around 6%. Thus, the LOI seems to be a good proxy for alteration grade. The K_2O and CaO values follow the same evolution that the LOI values, which confirms that illite and calcite are the main mineral phases of the argillic alteration in the wall rocks. Variation of the SiO_2 values is more erratic that of the K_2O, CaO, and LOI values due to the heterogeneous distribution of quartz veins.

4.4. Identification of Clay Minerals

The clay minerals in the GIL-1 well are dominated by potassic dioctahedral TOT (tetrahedral-octahedral-tetrahedral) clay minerals including illite and I/S ml, related either to argillic alteration in the vicinity of fractures (the dominant contribution) or to the propylitic alteration in the poorly altered granite in which chlorite and coarse grained illite replaced biotite and feldspars, respectively.
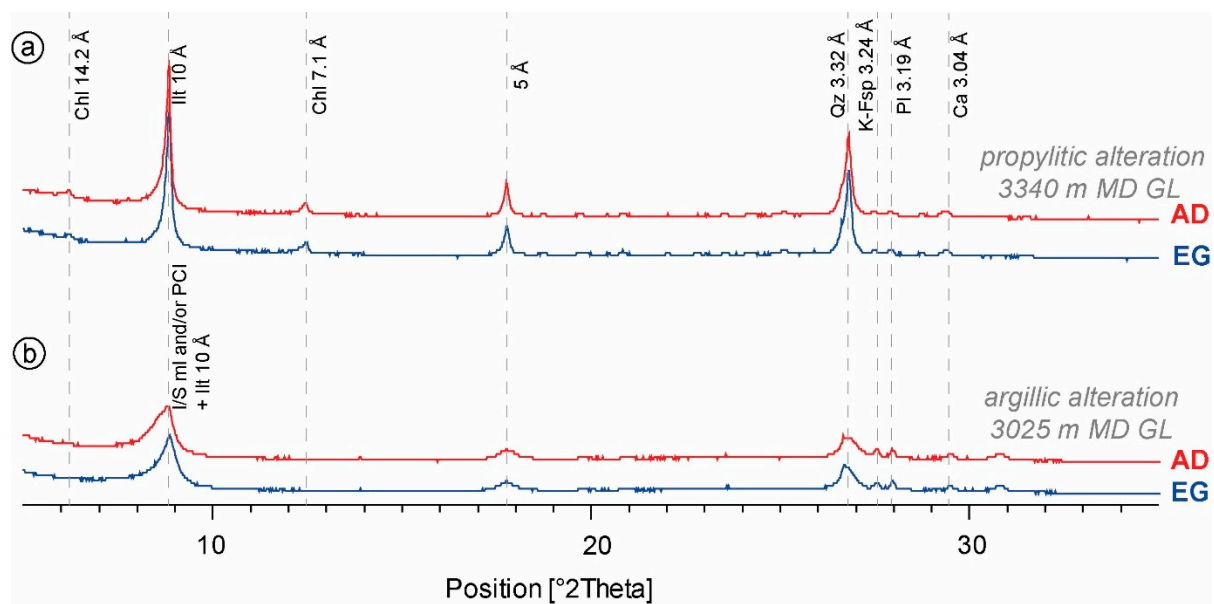
Figure 5. XRD results of oriented samples made on the fraction <5 μm from the GIL-1 well under air dried (AD) and ethylene-glycol (EG) conditions. (**a**) cutting sample at 3340 m MD in propylitic alteration, presenting a predominance of well crystallized illite (WCI) (+/− micas), (**b**) cutting sample at 3025 m MD in argillic alteration, presenting a predominance of I/S ml and PCI whereas the sample at Ca = calcite, Chl = chlorite, Ilt = illite, I/S ml = illite-rich illite-smectite mixed layers, K-Fsp = potassic feldspar, Pl = plagioclase, Qz = quartz.

4.4.1. Illite and Illite-Rich I/S ML

The XRD pattern of air-dried (AD) as well as ethylene-glycol (EG) saturated powder-prepared illite is characterized by the reflections at 10, 5, and 3.33 Å whereas, due to their swelling behavior, XRD reflections of illite-rich I/S ml slightly shift after EG saturation, resulting in asymmetrical broadening of the peak at 10 Å. As the XRD reflections of illite are similar to those of micas, a combination of several parameters such as the ratio I002/I001 and the FWHM of the peak at 10 Å can be used to differentiate illite from primary biotite.

The value of I002/I001 is lower than 0.10 for trioctahedral micas (biotite here), whereas dioctahedral clays (illite here) will have a value of I002/I001 between 0.37 and 0.55 [73] (Figure 3). Biotite was identified when the value of I002/I001 was lower than 0.10, and the full width at half maximum (FWHM) of the peak at 10 Å lower than 0.2° 2θ, suggesting the predominance of biotite (in the <5 μm fraction) in the zone from 3350 to 3433 m MD GL, consistent with the binocular observations (Figures 3 and 5). Biotite occurrence in the fine fraction is due to relics of biotite layers after incomplete chloritization, essentially in the propylitic altered zones (Figure 3b,c).

The FWHM calculated on the XRD reflection at 10 Å reflects crystallinity along the c axis. The FWHM of the peak at 10 Å higher or close to 0.2° 2θ is considered as a major contribution of illitic minerals [73] (Figure 3). Thus, the FWHM values ranging between 0.2 and 0.6 2Th indicated in the log (Figure 3) are indicative of the predominance of illite and/or illite rich I/S ml. The XRD patterns in Figure 5a show that illite is the main aluminous clay associated with the propylitic alteration as no swelling was observed after EG saturation. The deconvolution of the 10 Å peak in the sample at 3171 m MD (propylitic granite—Figure 6a,b) shows that this peak is in fact more complex including a well crystallized illite (WCI) contribution associated with a poorly crystallized illite (PCI) contribution (Figure 6a,b). The XRD of illitic minerals associated with argillic alteration displays broader peaks with a slight swelling behavior after EG saturation as illustrated by the peak at 10 Å in Figure 5b. The deconvolution of the peak at 10 Å for the sample affected by argillic alteration superimposed on propylitic alteration (3452 m MD) shows the presence of an I/S ml phase coexisting with WCI and PCI (Figure 6c,d). The deconvolution of the peak at

10 Å for the sample affected by argillic alteration (3071 m MD) indicates the coexistence of at least two I/S ml phases in addition to PCI (Figure 6e,f). These two I/S phases have their peaks around 10.91 Å (I/S ml_1) and 10.23 Å (I/S ml_2) under AD conditions and separate into two other peaks around 10.98 Å and 9.88 Å for the first phase (I/S ml_1) and around 10.45 Å and 9.93 Å for the second phase (I/S ml_2) (Figure 6e,f). Additionally, the existence of heterogeneous illites in terms of crystallinity (PCI and WCI) is consistent with the petrographic observations showing a fine-grained matrix postdating large illite crystals. The WCI contribution seems predominant in the propylitic illite (Figure 6a,b) whereas the PCI contribution predominates in the argillic illite (Figure 6c–f). The illitic minerals related to argillic alteration differ from those related to propylitic alteration by the presence of I/S mixed-layer minerals (Figure 6). It can be noted that the amount of I/S ml was significantly higher with at least two phases in the samples from the present KFZ (3071 m MD) than in those from the paleo KFZ with one phase (3452 m MD). The 00*l* peak positions of I/S ml were interpreted as the amount of smectite in the I/S ml did not exceed 10% [73].
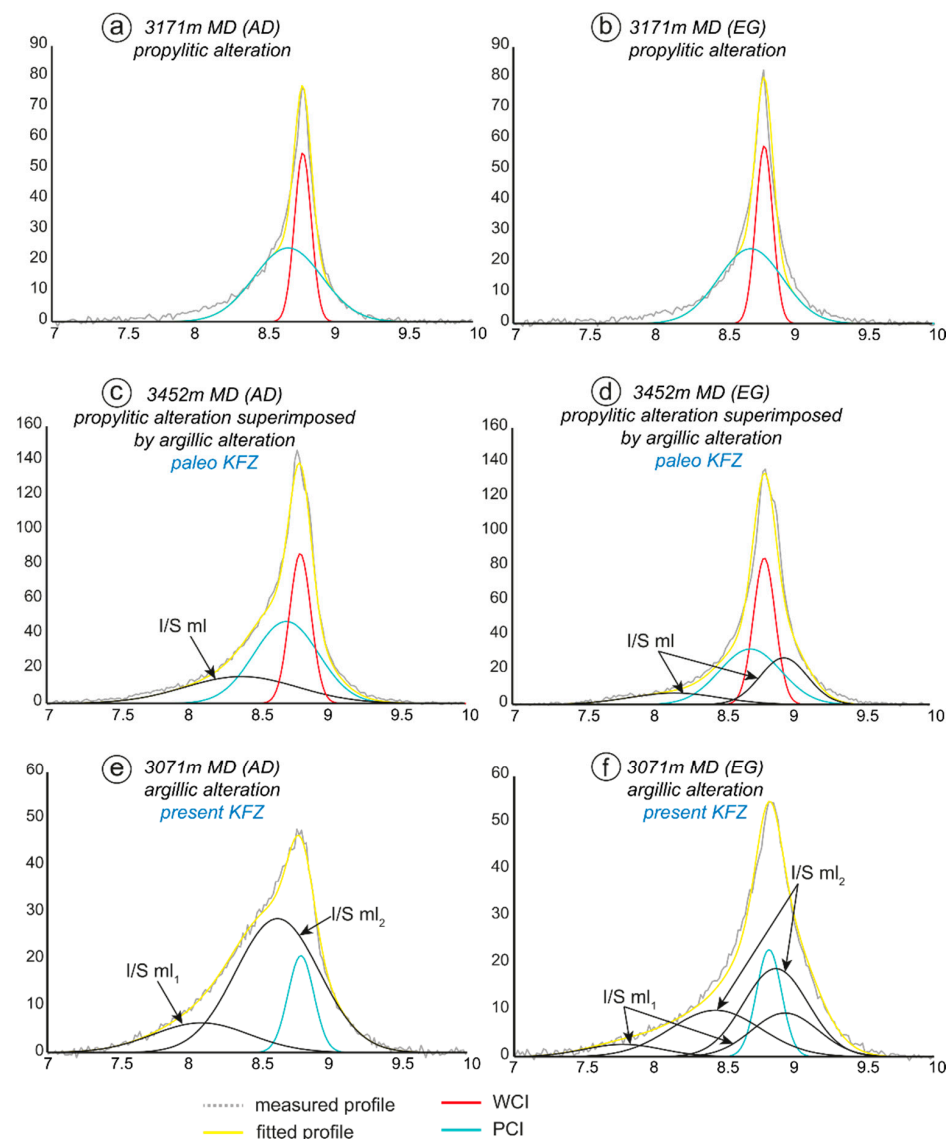

Figure 6. Decomposition of peak profile in the 7–10° 2θ CuKα domain of the x-ray diffractograms (<5 μm clay fraction) of air dry (AD) and ethylene glycol-saturated oriented powders (EG). (**a**) sample at 3171 m MD in AD, (**b**) sample at 3171 m MD in EG, (**c**) sample at 3452 m MD in AD, (**d**) sample at 3452 m MD in EG, (**e**) sample at 3071 m MD in AD, (**f**) sample at 3071 m MD in EG. I/S ml: illite-rich illite/smectite mixed layer; WCI: well crystallized illite, PCI: poorly crystallized illite.

In the GIL-1 well, the FWHM of the non-deconvoluted 10 Å peak varied with the grade of argillic alteration: at the top of the granite from 2984 to 3100 m MD where argillic alteration occurs, it was close to 0.28° 2Th, whereas in the weakly altered part of the granite from 3100 to 3800 m MD, the FWHM was of 0.182Th. Similarly, the highest values around 0.55 2Th were observed at 3026 and 3071 m MD in the argillic alteration whereas the lowest values around 0.13 2Th were observed in the biotite-rich granite (Figure 3a,c). This variation could be due to an increase of I/S ml contributions in argillic illitic minerals (as illustrated by the deconvoluted peaks Figure 6). No I/S ml were observed in the biotite-rich granite. Illite and more sparsely I/S ml, but similar to the one identified in the Illkirch well, were reported in the Rittershoffen [25] and Soultz-sous-Forêts wells [24,25,33,34,62,77–80].

4.4.2. Chlorite

Chlorite was identified as a non-expandable phyllosilicate with reflections at 14.2 Å, 7.1 Å, 3.73 Å, and 3.54 Å. The 001/002 ratio is homogeneous around 0.55, suggesting a homogeneous population of ferromagnesian chlorite (Figure 5). Chlorite is present in the predominantly propylitically altered granite from 3104 to 3800 m MD, with intensities of the 00*l* peak increasing with depth (Figure 3).

4.5. Chemical Compositions of Clay Minerals (EDS)
4.5.1. Illite and Illite-Rich I/S ML

Illite and I/S ml are generally characterized by an interlayer charge between 0.7 and 0.9 and lower than 0.7, respectively (Table 3 and Figure 4). Coupling SEM/EDX and XRD data confirm that the samples with interlayer charges lower than 0.7 contained I/S ml minerals in association with illite. However, due to the low smectite content of the I/S ml, the two populations of illitic minerals cannot be clearly distinguished from their chemical composition (Table 3).

Table 3. Oxides normalized on 100% and calculations of structural formulae of some illitic minerals at various depths in the GIL-1 well. Structural formulas were calculated relative to a structure containing 11 oxygen atoms and assuming that the total iron content is composed of Fe^{3+}. n.a.: number of analyses; An. Av.: analytical average; s.d.: standard deviation; OCT: octahedral occupancy; INTCH: interlayer charge; X_{Fe}: $Fe/(Fe + Mg + Mn)$. 2960, 3005 m MD: HHIG granite; 3071 m MD: KFZ1; 3340 m MD: KFZ4; 3482 m and 3573 m MD: HHIG granite on both sides of KFZ5; 3678 m MD: HLOW granite.

Samples n.a.	GIL-1 3005 m 67		GIL-1 3071 m 32		GIL-1 3340 m 18		GIL-1 3482 m 29		GIL-1 3573 m 29		GIL-1 3678 m 18		GIL-1 Rock 20	
	An. Av.	s.d.	An. Av.	s.d.	An. Av.	s.d.	An. Av.	s.d.	An. Av.	s.d.	An. Av.	s.d.	An. Av.	s.d.
SiO_2	52.11	1.44	52.56	1.44	52.40	1.41	52.03	1.06	53.34	1.87	52.57	1.03	53.71	1.59
Al_2O_3	33.02	2.51	32.26	2.63	30.58	1.35	32.90	1.86	31.37	1.94	32.47	0.97	30.81	1.83
Fe_2O_3	3.29	1.26	3.37	0.99	5.10	1.46	3.18	0.97	3.19	1.02	3.46	0.78	3.63	0.85
MgO	1.39	0.51	1.49	0.60	1.51	0.29	1.22	0.51	1.81	0.51	1.42	0.28	2.02	0.58
TiO_2	0.08	0.15	0.04	0.07	0.11	0.09	0.08	0.15	0.02	0.03	0.08	0.13	0.22	0.46
MnO	0.04	0.06	0.02	0.03	0.03	0.02	0.02	0.03	0.03	0.04	0.01	0.02	0.02	0.02
CaO	0.07	0.10	0.05	0.06	0.07	0.06	0.08	0.09	0.08	0.06	0.06	0.04	0.12	0.06
Na_2O	0.05	0.03	0.05	0.03	0.21	0.65	0.08	0.04	0.08	0.09	0.07	0.02	0.06	0.03
K_2O	9.95	0.74	10.15	0.65	10.00	1.13	10.42	0.38	10.09	0.57	9.88	0.36	9.42	0.53
Si	3.28	0.09	3.31	0.09	3.32	0.06	3.27	0.06	3.35	0.10	3.30	0.06	3.37	0.09
Al^{IV}	0.72	0.09	0.69	0.09	0.68	0.06	0.73	0.06	0.65	0.10	0.70	0.06	0.63	0.09
Al^{VI}	1.72	0.11	1.70	0.10	1.60	0.08	1.73	0.08	1.67	0.07	1.71	0.04	1.64	0.06
Fe^{3+}	0.16	0.06	0.16	0.05	0.24	0.07	0.15	0.05	0.15	0.05	0.16	0.04	0.17	0.04
Mg	0.13	0.05	0.14	0.06	0.14	0.03	0.11	0.05	0.17	0.05	0.13	0.03	0.19	0.05
Ti	0.00	0.01	0.00	0.00	0.01	0.00	0.00	0.01	0.00	0.00	0.00	0.01	0.01	0.02
Mn	0.00	0.00	0.00	0.00	0.00	0.00	0.00	0.00	0.00	0.00	0.00	0.00	0.00	0.00
OCT	2.01	0.03	2.00	0.03	1.99	0.02	1.99	0.01	2.00	0.03	2.01	0.02	2.01	0.02
Ca	0.00	0.01	0.00	0.00	0.00	0.00	0.01	0.01	0.01	0.00	0.00	0.00	0.01	0.00
Na	0.01	0.00	0.01	0.00	0.03	0.08	0.01	0.01	0.01	0.01	0.01	0.00	0.01	0.00
K	0.80	0.06	0.82	0.06	0.81	0.10	0.84	0.03	0.81	0.05	0.79	0.03	0.75	0.05
INTCH	0.81	0.06	0.83	0.05	0.84	0.04	0.86	0.03	0.83	0.05	0.81	0.03	0.78	0.04
XFe	0.54	0.09	0.53	0.10	0.63	0.08	0.56	0.09	0.47	0.12	0.55	0.08	0.48	0.12

The chemical composition of the illitic minerals analyzed from the GIL-1 well are reported in Table 3, indicating that tetrahedral substitutions range between 0.63 and 0.73 per half formula unit. Divalent cations in the octahedral sheet range from 0.10 to 0.17. In the intense argillic zone, illitic compositions show a small shift toward beidellite (Figure 7b,c) but the difference is minor and illitic minerals analyzed in the argillically or propylitically altered granites cannot be clearly distinguished by their chemical composition (Table 3 and Figure 7b,c). Compositionally, the illites from the Illkirch and Rittershoffen sites are similar, whereas illites from the Soultz-sous-Forêts site are closer to the illite pole (Figure 7a). Nevertheless, if we compare locally the chemical analyses of illitic minerals obtained as a function of their grain size, it appears that the chemical compositions of coarse grained illitic minerals, related to propylitic alteration, are closer to phengitic compositions. Coarse grained illitic minerals present higher interlayer charge (>0.85) (Figure 4b,d,f–h) compared to the superimposed fine-grained illitic minerals attributed to argillic alteration with lower interlayer charge (<0.85) (Figure 4d,g).
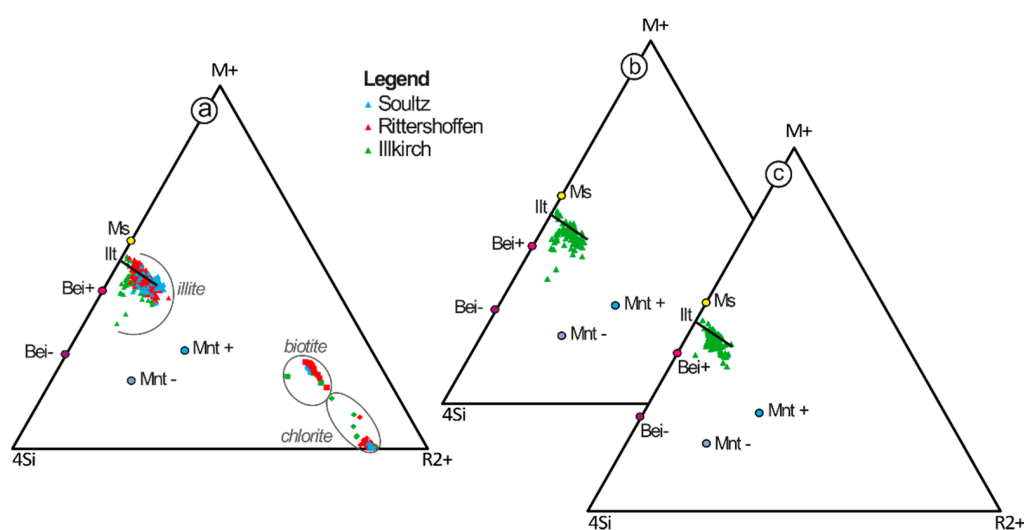

Figure 7. Chemical compositions of primary biotite, and illite and chlorite formed during the hydrothermal alteration of the granite at Soultz-sous-Forêts (GPK-1 well), Rittershoffen (GRT-1 and GRT-2 wells), and Illkirch (GIL-1 well) in the M+ 4Si R^{2+} diagram; (**a**) illites, biotites, and chlorite in the three sites, (**b**) illites in Illkirch granite affected by argillic fracture-related alteration (2894–2350 m MD); (**c**) illites in Illkirch granite affected by propylitic alteration (3104–3433 and 3513–3686 m MD); Bei +/−: beidellite high/low charge, Ilt: illite, Mnt +/−: montmorillonite high/low charge, Ms: muscovite. Soultz-sous-Forêts data are from [62] and Rittershoffen data are from [25].

4.5.2. Chlorite

The compositions of chlorite from Illkirch are homogeneous and comparable to those of chlorite in the propylitic zone in the Rittershoffen and Soultz-sous-Forêts fields (Table 4 and Figure 8) [25]. These compositions are controlled by the biotite compositions (Figure 8), with similar to slightly lower X_{Fe} values (due to Fe-Ti exsolution during the chloritization process). Chlorite in the GIL-1 well is ferro-magnesian with an average X_{Fe} value of 0.45 (Table 3, Figure 8). Small amounts of potassium as well as the low octahedral occupancy suggest an incomplete chloritization of the biotite layers (GIL-1 3482 m, 3340 m MD) (Table 4).

Table 4. Oxides normalized on 100% and calculations of structural formulae of some chlorite at various depths in the GIL-1 well. The structural formulas were calculated relative to a structure containing 14 oxygen and assuming that the total iron content is composed of Fe^{2+}. n.a.: number of analyses; An. Av.: analytical average; s.d.: standard deviation; OCT: octahedral occupancy; INTCH: interlayer charge; X_{Fe}: Fe/(Fe + Mg + Mn).

| Samples	GIL-1 3340 m	GIL-1 3482 m		GIL-1 3573 m		GIL-1 3678 m	
n.a.	1	2		9		3	
		An. Av.	s.d.	An. Av.	s.d.	An. Av.	s.d.
SiO_2	32.42	35.67	0.30	33.17	1.38	35.71	3.47
Al_2O_3	21.77	21.08	0.01	19.99	1.50	17.55	1.36
FeO	26.36	19.13	0.40	24.76	2.67	22.32	3.83
MgO	16.90	20.45	21.08	18.89	1.93	15.55	0.10
TiO_2	0	1.61	0.01	1.27	2.36	2.60	0.11
MnO	1.58	0.63	0.02	1.19	0.41	1.23	0.28
CaO	0.13	0.08	0.11	0.13	0.05	0.87	1.36
Na_2O	0.06	0.10	0.03	0.08	0.04	0.12	0.02
K_2O	0.77	1.26	0.14	0.52	0.77	4.06	3.33
Si	2.97	3.14	0.02	3.01	0.12	3.27	0.28
Al^{IV}	1.03	0.86	0.02	0.99	0.12	0.73	0.28
Al^{VI}	1.33	1.33	0.02	1.15	0.18	1.16	0.11
Fe^{2+}	2.02	1.41	0.03	1.91	0.25	1.71	0.32
Mg	2.31	2.68	0.01	2.55	0.20	2.12	0.04
Ti	0.00	0.11	0.00	0.09	0.16	0.18	0.01
Mn	0.12	0.05	0.00	0.09	0.03	0.10	0.02
OCT	5.79	5.57	0.01	5.79	0.16	5.27	0.26
Ca	0.01	0.01	0.01	0.01	0.01	0.09	0.14
Na	0.01	0.02	0.01	0.01	0.01	0.02	0.00
K	0.09	0.14	0.01	0.06	0.09	0.47	0.39
INTCH	0.13	0.17	0.01	0.10	0.09	0.66	0.12
XFe	0.45	0.34	0.01	0.42	0.04	0.43	0.04
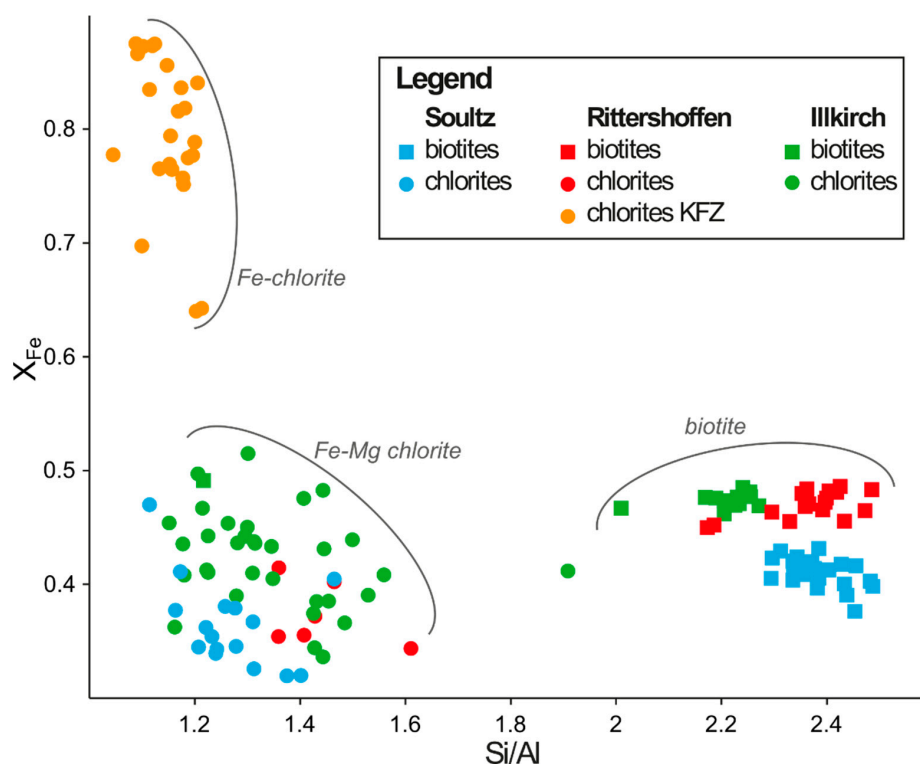
Figure 8. Plot of X_{Fe} (Fe/(Fe + Mg + Mn)) versus Si/Al content for the chlorite and biotite at Soultz-sous-Forêts, Rittershoffen, and Illkirch. Soultz-sous-Forêts data are from [62] and Rittershoffen data are from [25].

5. Discussion

5.1. Successive Hydrothermal Alterations in the Illkirch Reservoir

Two types of hydrothermal alteration events were distinguished in the Illkirch granitic basement. First, propylitic alteration developed pervasively in all the granitic basement during its post-magmatic cooling (Figure 9). It involved the partial chloritization of the primary biotite and a weak illitization of plagioclases in the GIL-1 well. Based on XRD and EDS analyses, chlorite composition clearly derives from biotite composition (Figure 8). This decrease in the ratio Si/Al between the biotite and the chlorite compositions is also observed at Soultz-sous-Forêts and Rittershoffen (Figure 8). From the SEM and EDS analyses, propylitic illitization is characterized by the occurrence of coarse-grained illite (WCI and PCI) with an interlayer charge higher than 0.85. According to [30,32,78,79], such a propylitic alteration is related to the resident hot and non-saline fluids equilibrating rapidly with the rock during the granite cooling, yielding a minimum age around 320 ± 8 Ma for the end of the propylitic alteration (maximum 10 Ma after the granite emplacement), and has been active in the granitic basement of the URG at temperatures higher than 350 °C and low fluid salinities (Figure 9) [32].

Second, in the GIL-1 well, argillic alteration is characterized by the precipitation of illitic minerals and carbonates in the vicinity of fractures and by secondary quartz veins related to fluid circulation in the fault cores (Figure 9). The major illitization stage comports small crystallites of illitic minerals (PCI, and I/S ml) with an interlayer charge lower than 0.85. The strong argillic alteration around the fracture networks replaces the primary minerals of the granite (biotite, feldspars) as well as the secondary minerals formed during the earlier propylitic alteration (chloritized biotite) by illitic minerals. Such a chemical process is more prevalent in the upper part of the well from 2894 to 3104 m MD (Figure 3a). This argillic alteration in the granitic basement of the URG occurred at temperatures between 130 and 160 °C and high fluid salinities close to the actual fluid conditions (100 g/L) (Figure 9) [32,56].

In the biotite-rich granite, the chlorite was preserved and no I/S ml were observed, reflecting a propylitic alteration in which WCI (well crystallized illite) was also observed as a slight early illitization occurring during and after the post-magmatic propylitic alteration (Figure 3). The biotite-rich granite is less hydrothermally altered than the porphyritic monzogranite. Hence, no major fractures cut the former rock, and an important small-scale fracture density was observed in the biotite-rich granite, which could be due to differences in mechanical properties between the two granitic bodies.

The propylitic alteration of the granite, related to the resident hot and non-saline fluids is supposed to occur at a minimum age around 320 ± 8 Ma, and temperatures higher than 350 °C [30,56,78,80]. The argillic alteration is related to the fluid circulation of a mix of meteoric water and brine of the NaCl type with TDS values close to 100 g/L, pH values close to 5.0, and K content of 3000–4000 ppm (Table 1) [56]. This fluid mix is constantly recharged, inducing a continuous argillic alteration [56,82,83]. The high content of K in the fluids is associated with the liberation of Al, likely originating from the destruction of the primary potassic feldspars and biotite facilitated the formation of illitic minerals. Albeit pervasively distributed, the argillic alteration is the result of pulses of fluid flows in the fracture network as inferred from the presence of at least two types of I/S ml in the argillically altered samples. These ephemeral pulses are most likely related to the development of the fracture networks in the granites and overlying sandstone, which were triggered by the Eschau fault or its splays. During the opening, a drop in the temperature and pressure of the damage zone led to the deposition of clay minerals and quartz that sealed the fractures. These cyclic crack-seal processes resulted in the successive crystallization of illite or I/S ml phases observed in the studied samples that have a close chemical composition in agreement with [56], which suggests a rather homogeneous chemical composition of the brine in the Soultz-sous-Forêts, Rittershoffen, and Landau sites in the URG. On a longer time scale, several episodes of illite precipitation in the fractures and in the host rock are evident of several hydrothermal events since the Permian,

followed by younger events during the Jurassic and Cretaceous [33,38]. The occurrence of at least six generations of secondary quartz in the EPS-1 well of Soultz-sous-Forêts also support this hypothesis [35]. Regardless of the precise ages, we can still affirm that several hydrothermal events occurred on a long timescale, made of a pulsated circulation occurring on a shorter timescale. The argillic alteration took place post-Triassic, as the hydrothermal fluids include a contribution of Triassic marine brines mixed with meteoric water and ore-forming fluids [40,49,52,56].

In the Illkirch reservoir, the above-mentioned fluid circulations were intensively enhanced during the Oligocene by the shearing of the steeply-dipping Eschau fault, which presents a vertical normal apparent offset of kilometric scale [29,84–86]. Although no dating of illitic minerals in the Illkirch reservoir is available, the intense argillic alteration in the footwall granitic compartment of the Eschau fault (from 2894 to 3104 m MD in the GIL-1 well) is related to the recent hydrothermal activity (late Paleogene period). In contrast, in the deepest part of the GIL-1 well, further away from the major fault and associated alteration halo, the minerals of propylitic alteration facies (chlorite) and those related to argillic alteration (illitic minerals) during the Permian to Jurassic periods could have been preserved. A detailed mineralogical study of a Mesozoic hydrothermal event on the Buntsandstein sandstone located in the southern Black Forest shows an illite assemblage (illite and I/S) dated at the end of the Jurassic (147 Ma) based on K-Ar dating of authigenic illite [87]. The most realistic hypothesis is that the propylitic (1) and Permian-Jurassic argillic (2) alterations are totally overprinted in the top of the well by the late Eocene to early Oligocene Eschau fault-related argillic alteration, whereas the relics of (1) and (2) are preserved in the deepest part of the well, further away from the Eschau fault system.
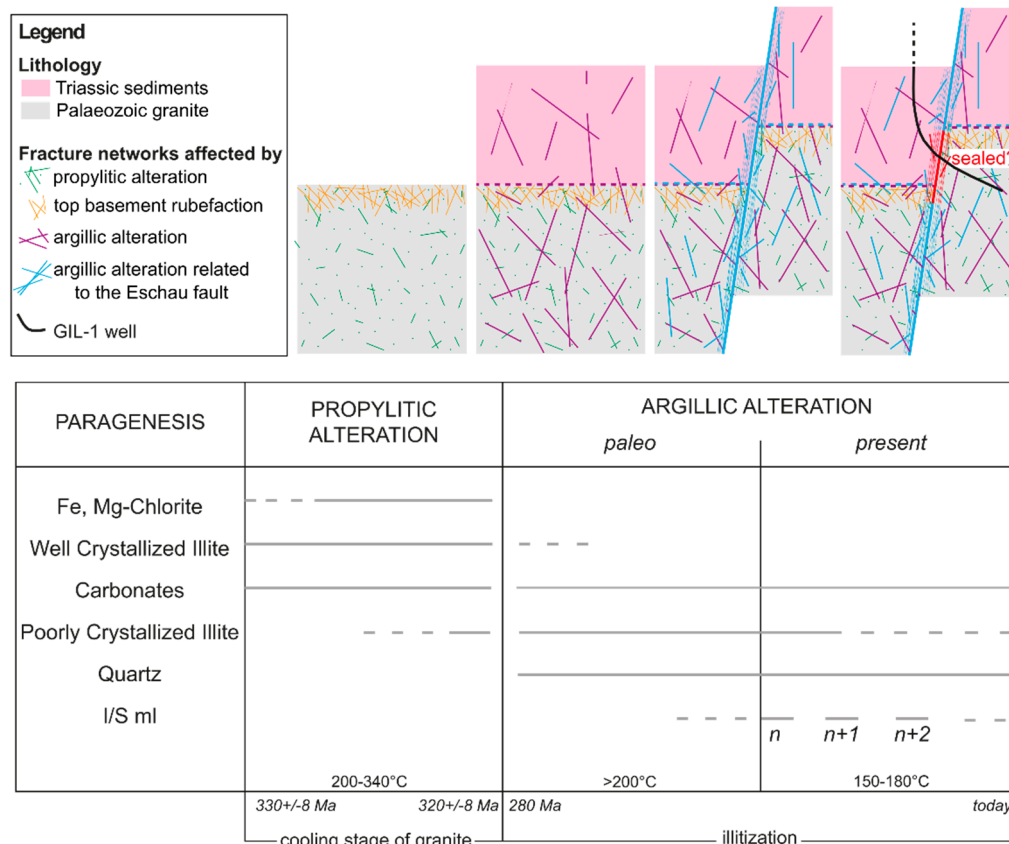

Figure 9. Paragenetic sequence of the granitic basement at Illkirch and schematic representation of the successive hydrothermal alterations that occurred in the fractured granite and sandstone intersected by the GIL-1 well at Illkirch. The top basement rubefaction was not observed at Illkirch because of the Eschau fault, but was observed at Soultz-sous-Forêts and Rittershoffen [88].

5.2. Successive Hydrothermal Alteration in the URG

The whole granitic basement of the URG underwent both propylitic and argillic alterations. In the three geothermal sites, the main mineralogical signature of the propylitic alteration is chlorite + carbonates $\pm$ epidote or hydrogrossular after biotite and amphibole and calcite + clay minerals after plagioclase [24,25,62,77]. If corrensite is quite common in Soultz-sous-Forêts in the replacement of plagioclases, it has never been identified in Rittershoffen or Illkirch [25]. In the latter site, the propylitic alteration produced coarse-grained WCI (+/−PCI), defined by quite a high interlayer charge (>0.85 per ^{11}O). In Soultz-sous-Forêts and in the Rittershoffen wells, epidote was observed [25,31], but has not been identified in Illkirch. Hydrogrossular has not been identified in both Rittershoffen and Illkirch sites, but is rare in Soultz-sous-Forêts. In all sites, primary potassic feldspar and quartz are preserved during propylitic alteration. Additionally, as the fluids are residents, the secondary mineralogy resulting from the propylitic alteration is constrained both by the chemical composition of the most reactive primary minerals of the granite and by the paleo-temperature.

In the three sites, the main mineralogical signature of the argillic alteration is the presence of illite and I/S ml, due to the illitization of primary plagioclase, potassic feldspar, biotite, and/or chloritized biotite. However, some differences are observed. In Soultz-sous-Forêts, the secondary minerals like quartz, carbonates (calcite, ankerite, dolomite), barite, tosudite, illite, and I/S ml, sulfides, hematite, and titanite accompany this illitization stage [24,89], while in Rittershoffen and Illkirch, the secondary minerals consist only of quartz, carbonates, anhydrite, and hematite [25,65]. The Rittershoffen site is mineralogically distinguished from the Illkirch and Soultz-sous-Forêts sites by the occurrence of additional Fe-chlorite.

The main differences in the argillic secondary mineralogy in the three sites are:

1. The occurrence of tosudite at Soultz-sous-Forêts, which could be related to the presence of organic compounds related to the overlying petroleum field [77];
2. The sparse occurrence of Fe-chlorite at Rittershoffen associated with reducing conditions and higher temperatures than those of the present-day [25,90]; and
3. The occurrence of barite at Soultz-sous-Forêts, compared to the occurrence of anhydrite at Rittershoffen and Illkirch, which could be related to the amount of Barium, liberated by the dissolution of feldspars under acidic conditions.

These small local disparities in the secondary mineralogy related to the argillic alteration seem mostly linked to the fluid properties. Hence, small changes in the chemical composition of the fluid (mixing rate between brine and meteoric waters) as well as its temperature are reflected in the secondary mineralogy, surely due to a reservoir with dynamic fluid circulation and precipitations in conditions of strong chemical disequilibrium. However, the main signature of argillic alteration in the URG, characterized by the presence of illite and I/S ml, is unchanged.

5.3. Towards an Argillic Signature in Permeable Fracture Zones

Previous studies in the Rittershoffen wells suggested that I/S ml are a proxy of the occurrence of KFZs [25]. In the Illkirch well, I/S ml are spatially associated with the occurrence of some KFZs (Figure 3). However, based on the three deconvoluted samples (Figure 6), the present-KFZ exhibits at least two I/S ml populations whereas the paleo-KFZs have one or more populations of I/S ml. This suggests a higher I/S ml content in the present-KFZs. Furthermore, the temperature needed for the formation of I/S ml is similar to the actual temperature (150 °C) measured in the GIL-1 well. This suggests that I/S ml could be coeval with the actual thermal regime. Hence, the amount of clay minerals formed during the argillic alteration of the granitic basement was heterogeneous as they showed several alteration grades (Figures 3 and 4, and Table 2). This suggests that the amount of secondary illitic minerals is enhanced by the quantity of fluid that has been circulating in the FZ, making more or less K available for the formation of secondary illitic minerals and more particularly I/S ml. This observation underscores the relation between

the alteration quantity and the fluid–rock ratio [91]. The flow quantity depends on the size of the fractured and damaged zone (permeability), the time during which the rock was exposed to the fluid, and the stress field [92].

As mentioned previously, only one KFZ is present in the upper part of the intensely argillically altered granite (first zone), which corresponds to the footwall of the Eschau fault (Figure 2). In contrast, five KFZs occur in the lower part of the propylitically altered (second zone) and biotite-rich granites; the above alteration is superimposed by moderate argillic alteration in the vicinity of the fault zone. From these observations, we propose that in the Illkirch granitic basement, the moderately argillically altered granite is situated >200 m from the Eschau fault. There, the permeability of the altered granite is greater than that of the intensely altered granite near the fault, because the latter is a sealed zone. Hence, the repartition of the illitic minerals' quantity in the granitic basement intersected by Soultz-sous-Forêts and Rittershoffen wells was reflected in the short-wave infrared spectroscopy (SWIR) patterns, which we interpreted to indicate the past and present fluid circulation [26,71,93,94]. In the Soultz-sous-Forêts and Rittershoffen wells, the SWIR data underlined that the KFZs are associated with high quantities of illitic minerals, suggesting a regular re-opening of the associated fractures [26,94]. SWIR was also applied to the Illkirch well and resolved the difference of permeability between the footwall granitic compartment of the Eschau fault and the deepest part of the well.

6. Conclusions

The newly drilled geothermal well at Illkirch provides an excellent opportunity to study the nature of the primary and secondary minerals of the granitic basement in the URG. Our findings show that the granitic basement, the hydrothermal alteration products, and the fluids circulating in the fractures/fault networks at Illkirch are similar to those at Soultz-sous-Forêts and Rittershoffen. Moreover, the repartition of the present-KFZs in the Illkirch well indicates that the moderately argillically altered granite distally situated from the Eschau fault is more permeable than the intensely argillically altered granite close to the Eschau fault.

The present-day fluid temperatures at Illkirch (150 °C) correspond with the occurrence of I/S ml rather than illite, which generally forms at temperatures ≥200 °C. This suggests that illite was probably associated with the paleo-KFZs but at higher temperature, and I/S ml to the present (or more recent)-KFZs but at lower temperature. Thus, the above temperature trend, as indicated by dioctahedral clay minerals, could be interpreted as a retrograde thermal system in this part of the Central URG. High quantities of I/S ml could be linked to present-KFZs. The heterogeneities of the illitic minerals (in terms of textural and structural properties) and the common superimposition of illite (WCI and PCI) with various populations of I/S ml point to several superimposed fluid/rock interaction events linked to the tectonic activities in the URG. Moreover, the Eschau fault targeted by the GIL-1 well was tight in the footwall, suggesting a pervasive and compact sealing by illitic minerals.

The similarities in the secondary mineralogy at the Illkirch, Soultz, and Rittershoffen basement granites suggest that fluid–rock interactions at the three sites operate under comparable pressure-temperature conditions and that the fluid chemistries are similar.

Clay mineralogy is a promising exploration tool for geothermal fields, hence the chemical composition, amount and species of clay minerals have recorded the paleo-fluid conditions and their zonation indicate the paleo and present-KFZs. Besides, more dating results could surely improve the interpretation of the characteristics of clay minerals in KFZs.

Author Contributions: C.G., P.P., J.V., A.G., and D.B.: Conceptualization, Methodology, Validation, Investigation, Writing-Review & Editing; C.G.: Data Acquisition and Curation, Software, Formal analysis, Writing-original draft preparation, Visualization; P.P. and A.G.: Resources, Supervision; A.G.: Project administration, Funding acquisition. All authors have read and agreed to the published version of the manuscript.

Data Availability Statement: Geophysical logs of the Illkirch well belong to ESIG. Please contact ES-Géothermie for data requests at geothermie@es.fr.

Conflicts of Interest: The funders had no role in the design of the study; in the collection, analyses, or interpretation of data; in the writing of the manuscript, or in the decision to publish the results.

References

1. Masanet, E.; Chang, Y.; Gopal, A.R.; Larsen, P.; Morrow, W.R.; Sathre, R.; Shehabi, A.; Zhai, P. Life-Cycle Assessment of Electric Power Systems. *Annu. Rev. Environ. Resour.* **2013**, *38*, 107–136. [CrossRef]
2. Pratiwi, A.; Ravier, G.; Genter, A. Life-Cycle Climate-Change Impact Assessment of Enhanced Geothermal System Plants in the Upper Rhine Valley. *Geothermics* **2018**, *75*, 26–39. [CrossRef]
3. Vidal, J.; Genter, A. Overview of Naturally Permeable Fractured Reservoirs in the Central and Southern Upper Rhine Graben: Insights from Geothermal Wells. *Geothermics* **2018**, *74*, 57–73. [CrossRef]
4. Baujard, C.; Genter, A.; Dalmais, E.; Maurer, V.; Hehn, R.; Rosillette, R.; Vidal, J.; Schmittbuhl, J. Hydrothermal Characterization of Wells GRT-1 and GRT-2 in Rittershoffen, France: Implications on the Understanding of Natural Flow Systems in the Rhine Graben. *Geothermics* **2017**, *65*, 255–268. [CrossRef]
5. Inoue, A. Formation of Clay Minerals in Hydrothermal Environments. In *Origin and Mineralogy of Clays*; Velde, B., Ed.; Springer: Berlin, Germany, 1995.
6. Beaufort, D.; Papapanagiotou, P.; Patrier, P.; Fouillac, A.M.; Traineau, H. *I/S and C/S Mixed Layers, Some Indicators of Recent Physical-Chemical Changes in Active Geothermal Systems: The Case Study of Chipilapa (El Salvador)*; Stanford University: Stanford, CA, USA, 1996.
7. Mas, A.; Guisseau, D.; Patrier Mas, P.; Beaufort, D.; Genter, A.; Sanjuan, B.; Girard, J.P. Clay Minerals Related to the Hydrothermal Activity of the Bouillante Geothermal Field (Guadeloupe). *J. Volcanol. Geotherm. Res.* **2006**, *158*, 380–400. [CrossRef]
8. Rigault, C.; Patrier, P.; Beaufort, D. Clay Minerals Related to Circulation of near Neutral to Weakly Acidic Fluids in Active High Energy Geothermal Systems. *Bull. Société Géologique Fr.* **2010**, *181*, 337–347. [CrossRef]
9. Buatier, M.D.; Chauvet, A.; Kanitpanyacharoen, W.; Wenk, H.R.; Ritz, J.F.; Jolivet, M. Origin and Behavior of Clay Minerals in the Bogd Fault Gouge, Mongolia. *J. Struct. Geol.* **2012**, *34*, 77–90. [CrossRef]
10. Lévy, L.; Fridriksson, T.; Findling, N.; Lanson, B.; Fraisse, B.; Marino, N.; Gibert, B. Smectite Quantification in Hydrothermally Altered Volcanic Rocks. *Geothermics* **2020**, *85*, 101748. [CrossRef]
11. Meunier, A. Superposition de deux altérations hydrothermales dans la syénite monzonitique du Bac de Montmeyre (Sondage INAG 1, Massif Central, France). *Bulmi* **1982**, *105*, 386–394. [CrossRef]
12. Kamineni, D.C.; Dugal, J.J.B. A Study of Rock Alteration in the Eye—Dashwa Lakes Pluton, Atikokan, Northwestern Ontario, Canada. *Chem. Geol.* **1982**, *36*, 35–57. [CrossRef]
13. Nishimoto, S.; Yoshida, H. Hydrothermal Alteration of Deep Fractured Granite: Effects of Dissolution and Precipitation. *Lithos* **2010**, *115*, 153–162. [CrossRef]
14. Storey, B.C.; Lintern, B.C. *Alteration, Fracture Infills and Weathering of the Strath Halladale Granite*; Institute of Geological Sciences: London, UK, 1981; p. 32.
15. Fulignati, P. Clay Minerals in Hydrothermal Systems. *Minerals* **2020**, *10*, 919. [CrossRef]
16. Peters, T.; Hofmann, B. Hydrothermal Clay Mineral Formation in a Biotite-Granite in Northern Switzerland. *Clay Miner.* **1984**, *19*, 579–590. [CrossRef]
17. Meunier, A.; Velde, B. Solid Solutions in I/S Mixed-Layer Minerals and Illite. *Am. Mineral.* **1989**, *74*, 1106–1112.
18. Genter, A.; Traineau, H.; Ledésert, B.; Bourgine, B.; Gentier, S. Over 10 Years of Geological Investigations within the HDR Soultz Project, France. In Proceedings of World Geothermal Congress, Kyushu, Japan, 28 May–10 June 2000; pp. 3707–3712.
19. Staněk, M.; Géraud, Y. Granite Microporosity Changes Due to Fracturing and Alteration: Secondary Mineral Phases as Proxies for Porosity and Permeability Estimation. *Solid Earth* **2019**, *10*, 251–274. [CrossRef]
20. Huang, W.L.; Bishop, A.M.; Brown, R.W. The Effect of Fluid/Rock Ratio on Feldspar Dissolution and Illite Formation under Reservoir Conditions. *Clay Miner.* **1986**, *21*, 585–601. [CrossRef]

21. Schmidt, R.B.; Bucher, K.; Stober, I. Experiments on Granite Alteration under Geothermal Reservoir Conditions and the Initiation of Fracture Evolution. *Eur. J. Mineral.* **2018**, *30*, 899–916. [CrossRef]

22. Drüppel, K.; Stober, I.; Grimmer, J.C.; Mertz-Kraus, R. Experimental Alteration of Granitic Rocks: Implications for the Evolution of Geothermal Brines in the Upper Rhine Graben, Germany. *Geothermics* **2020**, *88*, 101903. [CrossRef]

23. Gleeson, S.A.; Yardley, B.W.D. Extensional Veins and Pb-Zn Mineralisation in Basement Rocks: The Role of Penetration of Formation Brines. *Water-Rock Interact.* **2002**, *40*, 189–205. [CrossRef]

24. Ledésert, B.; Berger, G.; Meunier, A.; Genter, A.; Bouchet, A. Diagenetic-Type Reactions Related to Hydrothermal Alteration in the Soultz-Sous-Forets Granite, France. *Eur. J. Mineral.* **1999**, *11*, 731–741. [CrossRef]

25. Vidal, J.; Patrier, P.; Genter, A.; Beaufort, D.; Dezayes, C.; Glaas, C.; Lerouge, C.; Sanjuan, B. Clay Minerals Related to the Circulation of Geothermal Fluids in Boreholes at Rittershoffen (Alsace, France). *J. Volcanol. Geotherm. Res.* **2018**, *349*, 192–204. [CrossRef]

26. Glaas, C.; Vidal, J.; Patrier, P.; Girard, J.-F.; Beaufort, D.; Petit, S.; Genter, A. How Do Secondary Minerals in Granite Help Distinguish Paleo- from Present-Day Permeable Fracture Zones? Joint Interpretation of SWIR Spectroscopy and Geophysical Logs in the Geothermal Wells of Northern Alsace. *Geofluids* **2019**, *2019*, 1–20. [CrossRef]

27. Reinecker, J.; Hochschild, T.; Kraml, M.; Löschan, G.; Kreuter, H. Experiences and Challenges in Geothermal Exploration in the Upper Rhine Graben. In Proceedings of European Geothermal Congress, Den Haag, The Netherlans, 11–14 June 2019; p. 8.

28. Richard, A.; Maurer, V.; Edel, J.-B.; Genter, A.; Baujard, C.; Dalmais, E. Towards Targeting Geothermal Reservoir: Exploration Program for a New EGS Project in Urban Context in Alsace. In Proceedings of the European Geothermal Congress, Strasbourg, France, 19–24 September 2016; pp. 1–7.

29. Edel, J.B.; Maurer, V.; Dalmais, E.; Genter, A.; Richard, A.; Letourneau, O.; Hehn, R. Structure and Nature of the Palaeozoic Basement Based on Magnetic, Gravimetric and Seismic Investigations in the Central Upper Rhinegraben: Focus on the Deep Geothermal Project of Illkirch-Graffenstaden. *Geotherm. Energy* **2018**, *6*. [CrossRef]

30. Cocherie, A.; Guerrot, C.; Fanning, C.M.; Genter, A. Datation U–Pb Des Deux Faciès Du Granite de Soultz (Fossé Rhénan, France). *Comptes Rendus Geosci.* **2004**, *336*, 775–787. [CrossRef]

31. Stussi, J.-M.; Cheilletz, A.; Royer, J.-J.; Chèvremont, P.; Féraud, G. The Hidden Monzogranite of Soultz-Sous-Forêts (Rhine Graben, France). Mineralogy, Petrology and Genesis. *Géologie Fr.* **2002**, *1*, 45–64.

32. Dubois, M.; Ayt Ougougdal, M.; Meere, P.; Royer, J.-J.; Boiron, M.-C.; Cathelineau, M. Temperature of Paleo- to Modern Self-Sealing within a Continental Rift Basin: The Fluid Inclusion Data (Soultz-Sous-Forêts, Rhine Graben, France). *Eur. J. Mineral.* **1996**, *8*, 1065–1080. [CrossRef]

33. Schleicher, A.M.; Warr, L.N.; Kober, B.; Laverret, E.; Clauer, N. Episodic Mineralization of Hydrothermal Illite in the Soultz-Sous-Forêts Granite (Upper Rhine Graben, France). *Contrib Miner. Petrol* **2006**, *152*, 349–364. [CrossRef]

34. Bartier, D.L.; Meunier, A.; Liewig, N.; Morvan, G.; Addad, A. Hydrothermal Alteration of the Soultz-Sous-Forets Granite (Hot Fractured Rock Geothermal Exchanger) into a Tosudite and Illite Assemblage. *Eur. J. Mineral.* **2008**, *20*, 131–142. [CrossRef]

35. Smith, M.P.; Savary, V.; Yardley, B.W.D.; Valley, J.W.; Royer, J.J.; Dubois, M. The Evolution of the Deep Flow Regime at Soultz-sous-Forêts, Rhine Graben, Eastern France: Evidence from a Composite Quartz Vein. *J. Geophys. Res. Solid Earth* **1998**, *103*, 27223–27237. [CrossRef]

36. Duringer, P.; Aichholzer, C.; Orciani, S.; Genter, A. The Complete Lithostratigraphic Section of the Geothermal Wells in Rittershoffen (Upper Rhine Graben, Eastern France): A Key for Future Geothermal Wells. *BSGF Earth Sci. Bull.* **2019**, *190*, 13. [CrossRef]

37. GeOrg, T. EU-Projekt GeORG—Geoportal. Available online: http://www.geopotenziale.org/home?lang=3 (accessed on 5 October 2020).

38. Bossennec, C.; Geraud, Y.; Bertrand, L.; Mattioni, L.; Moretti, I. Insights on Fluid Sources and Pathways in Geothermal Sandstone Reservoir by Structural and Geochemical Characterization of Fractures Infills. In Proceedings of World Geothermal Congress, Reykjavik, Iceland, March–October 2020; p. 12.

39. Baatartsogt, B.; Schwinn, G.; Wagner, T.; Taubald, H.; Beitter, T.; Markl, G. Contrasting Paleofluid Systems in the Continental Basement: A Fluid Inclusion and Stable Isotope Study of Hydrothermal Vein Mineralization, Schwarzwald District, Germany. *Geofluids* **2007**, *7*, 123–147. [CrossRef]

40. Burisch, M.; Gerdes, A.; Walter, F.B.; Neumann, U.; Fettel, M.; Markl, G. Methane and the Origin of Five-Element Veins: Mineralogy, Age, Fluid Inclusion Chemistry and Ore Forming Processes in the Odenwald, SW Germany. *Ore Geol. Rev.* **2017**, *81*, 42–61. [CrossRef]

41. Walter, B.F.; Burisch, M.; Markl, G. Long-Term Chemical Evolution and Modification of Continental Basement Brines—A Field Study from the Schwarzwald, SW Germany. *Geofluids* **2016**, *16*, 604–623. [CrossRef]

42. Dezayes, C.; Lerouge, C. Reconstructing Paleofluid Circulation at the Hercynian Basement/Mesozoic Sedimentary Cover Interface in the Upper Rhine Graben. *Geofluids* **2019**, *2019*, 1–30. [CrossRef]

43. Clauer, N.; Liewig, N.; Ledesert, B.; Zwingmann, H. Thermal History of Triassic Sandstones from the Vosges Mountains-Rhine Graben Rifting Area, NE France, Based on K-Ar Illite Dating. *Clay Miner.* **2008**, *43*, 363–379. [CrossRef]

44. Lippolt, H.J.; Seibel, W. Evidence for Multistage Alteration of Schwarzwald Lamprophyres. *Eur. J. Mineral.* **1991**, *3*, 587–601. [CrossRef]

45. Burisch, M.; Walter, B.F.; Gerdes, A.; Lanz, M.; Markl, G. Late-Stage Anhydrite-Gypsum-Siderite-Dolomite-Calcite Assemblages Record the Transition from a Deep to a Shallow Hydrothermal System in the Schwarzwald Mining District, SW Germany. *Geochim. Cosmochim. Acta* **2017**, *223*, 259–278. [CrossRef]

46. Pfaff, K.; Hildenbrandt, L.H.; Leach, D.L.; Jacob, D.E.; Markl, G. Formation of the Wiesloch Mississippi Valley-Type Zn-Pb-Ag Deposit in the Extensional Setting of the Upper Rhinegraben, SW Germany. *Mineral Deposits* **2010**, *45*, 647–666. [CrossRef]

47. Walter, B.F.; Burisch, M.; Marks, M.A.W.; Markl, G. Major Element Compositions of Fluid Inclusions from Hydrothermal Vein-Type Deposits Record Eroded Sedimentary Units in the Schwarzwald District, SW Germany. *Miner. Depos.* **2017**, *52*, 1191–1204. [CrossRef]

48. Cathelineau, M.; Boiron, M.-C.; Fourcade, S.; Ruffet, G.; Clauer, N.; Belcourt, O.; Coulibaly, Y.; Banks, D.A.; Guillocheau, F. A Major Late Jurassic Fluid Event at the Basin/Basement Unconformity in Western France: 40Ar/39Ar and K–Ar Dating, Fluid Chemistry, and Related Geodynamic Context. *Chem. Geol.* **2012**, *322–323*, 99–120. [CrossRef]

49. Walter, B.F.; Kortenbruck, P.; Scharrer, M.; Zeitvogel, C.; Wälle, M.; Mertz-Kraus, R.; Markl, G. Chemical Evolution of Ore-Forming Brines—Basement Leaching, Metal Provenance, and the Redox Link between Barren and Ore-Bearing Hydrothermal Veins. A Case Study from the Schwarzwald Mining District in SW-Germany. *Chem. Geol.* **2019**, *506*, 126–148. [CrossRef]

50. Bons, P.D.; Fusswinkel, T.; Gomez-Rivas, E.; Markl, G.; Wagner, T.; Walter, B. Fluid Mixing from below in Unconformity-Related Hydrothermal Ore Deposits. *Geology* **2014**, *42*, 1035–1038. [CrossRef]

51. Staude, S.; Mordhorst, T.; Nau, S.; Pfaff, K.; Brügmann, G.; Jacob, D.E.; Markl, G. Hydrothermal Carbonates of the Schwarzwald Ore District, Southwestern Germany: Carbon Source and Conditions of Formation Using Delta18O, Delta13C, 87Sr/86Sr, and Fluid Inclusions. *Can. Mineral.* **2012**, *50*, 1401–1434. [CrossRef]

52. Walter, B.F.; Burisch, M.; Fusswinkel, T.; Marks, M.A.W.; Steele-MacInnis, M.; Wälle, M.; Apukhtina, O.B.; Markl, G. Multi-Reservoir Fluid Mixing Processes in Rift-Related Hydrothermal Veins, Schwarzwald, SW-Germany. *J. Geochem. Explor.* **2018**, *186*, 158–186. [CrossRef]

53. Boiron, M.-C.; Cathelineau, M.; Richard, A. Fluid Flows and Metal Deposition near Basement/Cover Unconformity: Lessons and Analogies from Pb-Zn-F-Ba Systems for the Understanding of Proterozoic U Deposits. *Geofluids* **2010**, *10*, 270–292. [CrossRef]

54. Cathelineau, M.; Fourcade, S.; Clauer, N.; Buschaert, S.; Rousset, D.; Boiron, M.-C.; Meunier, A.; Lavastre, V.; Javoy, M. Dating Multistage Paleofluid Percolations: A K-Ar and 18O/16O Study of Fracture Illites from Altered Hercynian Plutonites at the Basement/Cover Interface (Poitou High, France). *Geochim. Cosmochim. Acta* **2004**, *68*, 2529–2542. [CrossRef]

55. Schwinn, G.; Wagner, T.; Baatartsogt, B.; Markl, G. Quantification of Mixing Processes in Ore-Forming Hydrothermal Systems by Combination of Stable Isotope and Fluid Inclusion Analyses. *Geochim. Cosmochim. Acta* **2006**, *70*, 965–982. [CrossRef]

56. Sanjuan, B.; Millot, R.; Innocent, C.; Dezayes, C.; Scheiber, J.; Brach, M. Major Geochemical Characteristics of Geothermal Brines from the Upper Rhine Graben Granitic Basement with Constraints on Temperature and Circulation. *Chem. Geol.* **2016**, *428*, 27–47. [CrossRef]

57. Bosia, C.; Mouchot, J.; Ravier, G.; Seibel, O.; Genter, A. Evolution of Brine Geochemical Composition During Operation of EGS Geothermal Plants (Alsace, France). In Proceedings of the 46th Workshop on Geothermal Reservoir Engineering, Stanford University, Stanford, CA, USA, 15 February 2021; p. 21.

58. Sanjuan, B.; Négrel, G.; Lous, M.L.; Poulmarch, E.; Gal, F.; Damy, P.-C. Main Geochemical Characteristics of the Deep Geothermal Brine at Vendenheim (Alsace, France) with Constraints on Temperature and Fluid Circulation. In Proceedings of the Proceedings World Geothermal Congress 2021, Reykjavik, Iceland, 24–27 October 2021; p. 12.

59. Sanjuan, B.; Millot, R.; Dezayes, C.; Brach, M. Main Characteristics of the Deep Geothermal Brine (5 km) at Soultz-Sous-Forêts (France) Determined Using Geochemical and Tracer Test Data. *Comptes Rendus Geosci.* **2010**, *342*, 546–559. [CrossRef]

60. Parneix, J.-C.; Meunier, A. Les Transformations et La Microfissuration Du Granite de Mayet-de-Montagne (Allier, France) Sous l'influence Des Réactions Minérales d'altération. *Hydrothermale* **1982**, *38*, 203–210.

61. Chèvremont, P.; Genter, A. *Etude Pétrologique Des Échantillons de Granite de Soultz-Sous-Forêts, Forage GPK-1. IRG report*; Bureau De Recherches Geologiques Et Minieres: Orléans, France, 1989; p. 20.

62. Genter, A. Géothermie Roches Chaudes Sèches: Le Granite de Soultz-Sous-Forêts (Bas-Rhin, France). Fracturation Naturelle, Altérations Hydrothermales et Interaction Eau-Roche. Ph.D.Thesis, Université d'Orléans, Orléans, France, 1989.

63. Baillieux, P.; Schill, E.; Abdelfettah, Y.; Dezayes, C. Possible Natural Fluid Pathways from Gravity Pseudo-Tomography in the Geothermal Fields of Northern Alsace (Upper Rhine Graben). *Geotherm Energy* **2014**, *2*, 16. [CrossRef]

64. Traineau, H.; Genter, A.; Cautru, J.-P.; Fabriol, H.; Chèvremont, P. Petrography of the granite massif from drill cutting analysis and well log interpretation in the geothermal HDR borehole GPK-1 (Soultz, Alsace, France). *Geotherm. Sci. Technol.* **1992**, *3*, 1–29.

65. Glaas, C.; Genter, A.; Girard, J.F.; Patrier, P.; Vidal, J. How Do the Geological and Geophysical Signatures of Permeable Fractures in Granitic Basement Evolve after Long Periods of Natural Circulation? Insights from the Rittershoffen Geothermal Wells (France). *Geotherm. Energy* **2018**, *6*. [CrossRef]

66. Dezayes, C.; Genter, A.; Valley, B. Structure of the Low Permeable Naturally Fractured Geothermal Reservoir at Soultz. *Comptes Rendus Geosci.* **2010**, *342*, 517–530. [CrossRef]

67. Barton, C.A.; Zoback, M.D.; Moos, D. Fluid Flow along Potentially Active Faults in Crystalline Rock. *Geology* **1995**, *23*, 683–686. [CrossRef]

68. Davatzes, N.C.; Hickman, S.H. *Controls on Fault-Hosted Fluid Flow; Preliminary Results from the Coso Geothermal Field, CA*; Geothermal Resources Council: Davis, CA, USA, 2005; Volume 29, pp. 343–348.

69. Bradford, J.; McLennan, J.; Moore, J.; Glasby, D.; Waters, D.; Kruwells, R.; Bailey, A.; Rickard, W.; Bloomfield, K.; King, D. *Recent Developments at the Raft River Geothermal Field*; Stanford University: Stanford, CA, USA, 2013.

70. Vidal, J.; Hehn, R.; Glaas, C.; Genter, A. How Can Temperature Logs Help Identify Permeable Fractures and Define a Conceptual Model of Fluid Circulation? An Example from Deep Geothermal Wells in the Upper Rhine Graben. *Geofluids* **2019**, 14. [CrossRef]

71. Kraal, K.O.; Ayling, B.F.; Blake, K.; Hackett, L.; Perdana, T.S.P.; Stacey, R. Linkages between Hydrothermal Alteration, Natural Fractures, and Permeability: Integration of Borehole Data for Reservoir Characterization at the Fallon FORGE EGS Site, Nevada, USA. *Geothermics* **2021**, *89*, 101946. [CrossRef]

72. Carignan, J.; Hild, P.; Mevelle, G.; Morel, J.; Yeghicheyan, D. Routine Analyses of Trace Elements in Geological Samples Using Flow Injection and Low Pressure On-line Liquid Chromatography Coupled to ICP-MS: A Study of Geochemical Reference Materials BR, DR-N, UB-N, AN-G and GH. *Geostand. Newsl.* **2001**, *25*, 187–198. [CrossRef]

73. Brindley, G.W.; Brown, G. X-Ray Diffraction Procedures for Clay Mineral Identification. In *Crystal Structures of Clay Minerals and Their X-Ray Identification*; Brindley, G.W., Brown, G., Eds.; European Mineralogical Union: London, UK, 1980; Volume 5.

74. Moore, D.M.; Reynolds, R.C. *X-Ray Diffraction and the Identification and Analysis of Clay Minerals*, 2nd ed.; Oxford University Press: Oxford, UK; New York, NY, USA, 1997.

75. Wojdyr, M. Fityk: A General-Purpose Peak Fitting Program. *J. Appl. Crystallogr.* **2010**, *43*, 1126–1128. [CrossRef]

76. Genter, A.; Traineau, H. *Deepening of GPK-1 HDR Borehole 2000–3600 m (Soultz-Sous-Forêts). Geological Monitoring*; BRGM: Orléans, France, 1993.

77. Ledésert, B.; Joffre, J.; Amblès, A.; Sardini, P.; Genter, A.; Meunier, A. Organic Matter in the Soultz HDR Granitic Thermal Exchanger (France): Natural Tracer of Fluid Circulations between the Basement and Its Sedimentary Cover. *J. Volcanol. Geotherm. Res.* **1996**, *70*, 235–253. [CrossRef]

78. Ledésert, B.; Hebert, R.; Genter, A.; Bartier, D.; Clauer, N.; Grall, C. Fractures, Hydrothermal Alterations and Permeability in the Soultz Enhanced Geothermal System. *Comptes Rendus Geosci.* **2010**, *342*, 607–615. [CrossRef]

79. Jacquemont, B. Etude Des Interactions Eaux-Roches Dans Le Granite de Soultz-Sous-Forêts. Quantification et Modélisation Des Transferts de Matière Par Les Fluides. Ph.D. Thesis, Université de Strasbourg, Strasbourg, France, 2002.

80. Gardien, V.; Rabinowicz, M.; Vigneresse, J.-L.; Dubois, M.; Boulvais, P.; Martini, R. Long-Lived Interaction between Hydrothermal and Magmatic Fluids in the Soultz-Sous-Forêts Granitic System (Rhine Graben, France). *Lithos* **2016**, *246–247*, 110–127. [CrossRef]

81. Wilson, M.J. *Rock-Forming Minerals, Volume 3C, Sheet Silicates: Clay Minerals*; Geological Society: London, UK, 2013; Volume 3c, ISBN 978-1-86239-359-2.

82. Freymark, J.; Bott, J.; Cacace, M.; Ziegler, M.; Scheck-Wenderoth, M. Influence of the Main Border Faults on the 3D Hydraulic Field of the Central Upper Rhine Graben. *Geofluids* **2019**, *2019*, 1–21. [CrossRef]

83. Koltzer, N.; Scheck-Wenderoth, M.; Bott, J.; Cacace, M.; Frick, M.; Sass, I.; Fritsche, J.-G.; Bär, K. The Effects of Regional Fluid Flow on Deep Temperatures (Hesse, Germany). *Energies* **2019**, *12*, 2081. [CrossRef]

84. Doebl, F. The Tertiary and Pleistocene Sediments of the Northern and Central Part of the Upper Rhinegraben. *Abh. Geol. Landesans.* **1967**, *6*, 48–54.

85. Villemin, T.; Bergerat, F. L'évolution Structurale Du Fossé Rhénan Au Cours Du Cénozoïque: Un Bilan de La Déformation et Des Effets Thermiques de l'extension. *Bull. Soc. Géol. Fr.* **1987**, *8*, 245–255. [CrossRef]

86. Schumacher, M.E. Upper Rhine Graben: Role of Preexisting Structures during Rift Evolution. *Tectonics* **2002**, *21*, 6-1–6-17. [CrossRef]

87. Brockamp, O.; Schlegel, A.; Clauer, N. Mesozoic Hydrothermal Impact on Rotliegende and Bunter Immature Sandstones of the High Rhine Trough and Its Adjacent Eastern Area (Southern Black Forest, Germany). *Sediment. Geol.* **2011**, *234*, 76–88. [CrossRef]

88. Just, J.; Kontny, A. Thermally Induced Alterations of Minerals during Measurements of the Temperature Dependence of Magnetic Susceptibility: A Case Study from the Hydrothermally Altered Soultz-Sous-Forêts Granite, France. *Int. J. Earth Sci.* **2011**, *21*. [CrossRef]

89. Genter, A.; Traineau, H. Analysis of Macroscopic Fractures in Granite in the HDR Geothermal Well EPS-l, Soultz-Sous-Forêts, France. *J. Volcanol. Geotherm. Res.* **1996**, *72*, 121–141. [CrossRef]

90. Beaufort, D.; Rigault, C.; Billon, S.; Billault, V.; Inoue, A.; Inoue, S.; Patrier, P. Chlorite and Chloritization Processes through Mixed-Layer Mineral Series in Low-Temperature Geological Systems—A Review. *Clay Miner.* **2015**, *50*, 497–523. [CrossRef]

91. Komninou, A.; Yardley, B.W.D. Fluid-Rock Interactions in the Rhine Graben: A Thermodynamic Model of the Hydrothermal Alteration Observed in Deep Drilling. *Geochim. Cosmochim. Acta* **1997**, *61*, 515–531. [CrossRef]

92. Bruhn, R.L.; Parry, W.T.; Yonkee, W.A.; Thompson, T. Fracturing and Hydrothermal Alteration in Normal Fault Zones. *Pure Appl. Geophys.* **1994**, *142*, 36. [CrossRef]

93. Simpson, M.P.; Rae, A.J. Short-Wave Infrared (SWIR) Reflectance Spectrometric Characterisation of Clays from Geothermal Systems of the Taupō Volcanic Zone, New Zealand. *Geothermics* **2018**, *73*, 74–90. [CrossRef]

94. Glaas, C.; Vidal, J.; Patrier, P.; Beaufort, D.; Genter, A. Contribution of SWIR to the Clay Signature of Permeable Fracture Zones in the Granitic Basement. Overview of Soultz and Rittershoffen Wells. In Proceedings of European Geothermal Congress, Den Haag, The Netherlands, 11–14 June 2019; p. 11.